Photonic band structure calculations using scattering matrices

L. C. Botten
School of Mathematical Sciences, University of Technology, Sydney, New South Wales 2007, Australia

N. A. Nicorovici, R. C. McPhedran, C. Martijn de Sterke, and A. A. Asatryan
School of Physics, University of Sydney, New South Wales 2006, Australia

(Received 12 April 2001; published 20 September 2001)

We consider band structure calculations of two-dimensional photonic crystals treated as stacks of one-dimensional gratings. The gratings are characterized by their plane wave scattering matrices, the calculation of which is well established. These matrices are then used in combination with Bloch's theorem to determine the band structure of a photonic crystal from the solution of an eigenvalue problem. Computationally beneficial simplifications of the eigenproblem for symmetric lattices are derived, the structure of eigenvalue spectrum is classified, and, at long wavelengths, simple expressions for the positions of the band gaps are deduced. Closed form expressions for the reflection and transmission scattering matrices of finite stacks of gratings are established. A new, fundamental quantity, the reflection scattering matrix, in the limit in which the stack fills a half space, is derived and is used to deduce the effective dielectric constant of the crystal in the long wavelength limit.

DOI: 10.1103/PhysRevE.64.046603 PACS number(s): 42.25.Fx, 02.70.Hm, 78.20.Bh, 78.20.Ci

I. INTRODUCTION

Photonic crystals are structures in which the refractive index varies periodically with position. Their unprecedented ability to steer the propagation of light makes them prominent candidates to be the technology underpinning novel classes of photonic devices. An important tool in the modeling of photonic crystals is the band structure, which indicates how the propagation of light depends on frequency, polarization, and direction. For some photonic crystals, all traveling wave solutions are forbidden for a particular frequency interval, which is then referred to as a (complete) band gap. There exists a mature literature on the calculation of photonic band structures [1], with various approaches such as plane wave methods [2,3], transfer matrix method [4,5], finite difference time domain method [6], layer Korringa-Kohn-Rostoker method [7] and multipole methods [8,9]. Here, we introduce a generic method for calculating the band structure of two-dimensional photonic crystals, based upon the observation that such crystals can be considered as a stack of identical one-dimensional layers, each of which is a periodic diffraction grating. The scattering matrices of the gratings are used in combination with Bloch's theorem to determine the band structure of the crystal in a way first developed by McRae [10] for electron diffraction, and applied recently to the photonic crystal problem [7,11] In this way, band structure calculations can use any technique from the substantial literature on scattering by diffraction gratings [12,13].

There are a number of features in the treatment presented here that generalize the earlier work [10,11]. We take advantage of the symmetry that is present in rectangular, centered rectangular, and hexagonal crystals [14] to develop the eigenvalue problem in a form improved in both computational stability and efficiency. In fact, starting from a plane characterized by the Miller indices $[h_1 h_2]$, the method can be used to generate the band structure in the $[h_1 h_2]$ direction in the Brillouin zone, though here we only apply this to the usual high-symmetry directions.

We study not only propagating modes, but also the evanescent states. We also deduce the reflection and transmission matrices corresponding to a finite stack of gratings, and construct the limit of the reflection matrix to deduce $\mathbf{R}_\infty$, the reflection matrix of a semi-infinite space composed of stacked gratings. It is shown that this is a useful tool in studies of homogenization, i.e., the replacement of the crystal by an equivalent homogeneous dielectric. Finally, we discuss the occurrence of band gaps at long wavelengths, presenting a simple criterion for the onset of a band gap, and comment on the behavior of the photonic crystal near the edges of band gaps.

We formulate the method for the most general two-dimensional Bravais lattice, and give examples for the high-symmetry square and hexagonal lattices. Part of the formulation is an investigation of the pairing properties of the Bloch factors. Though the reflection and transmission matrices can be obtained in a variety of ways, here we use the multipole method for cylinder gratings described earlier by us [15,16]. Since multipole methods rely on the knowledge of lattice sums, our approach, in which we consider a two-dimensional structure to be built up from one-dimensional gratings, leads to relations between lattice sums of one- and two-dimensional lattices.

II. THE EIGENVALUE PROBLEM

A. Nomenclature

We consider an infinite periodic structure comprising identical layers, each of which is a one-dimensional diffraction grating, consisting of regular cylindrical inclusions of infinite extent in the z direction, in an otherwise uniform background medium. The basis vectors of the lattice are $\mathbf{e}_1 = d_1(1,0)$ and $\mathbf{e}_2 = d_2(\cos\psi, \sin\psi)$, with a general lattice vector being

$$\mathbf{l}_{mn} = m\mathbf{e}_1 + n\mathbf{e}_2 . \tag{1}$$

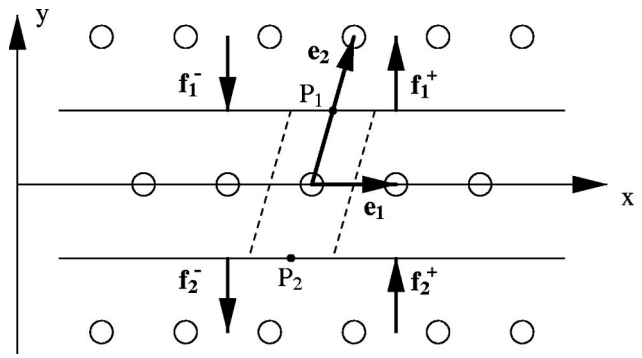

FIG. 1. Geometry of the unit cell (defined by the fundamental translation vectors $\mathbf{e}_1$ and $\mathbf{e}_2$) for the Bloch method calculations. The phase origins P_1 and P_2 of the fields respectively above ($\mathbf{f}_1^+$, $\mathbf{f}_1^-$) and below ($\mathbf{f}_2^+$, $\mathbf{f}_2^-$) the grating are shown.

For convenience, we introduce some additional nomenclature: $d_x = d_1$ denoting the period in the x-direction, $d_y = d_2 \sin\psi$ denoting the vertical displacement of successive gratings in the lattice, and $s_x = d_2 \cos\psi$ denoting the lateral shift of one grating relative to the next. For a square lattice we have $d_1 = d_2 = d$ and $\psi = \pi/2$, so that $d_x = d_y = d$ and $s_x = 0$, while for a hexagonally closed packed lattice $d_x = d$, $d_y = d\sqrt{3}/2$ and $s_x = d/2$ (i.e., $d_1 = d_2 = d$ and $\psi = \pi/6$). A schematic diagram for a general array is shown in Fig. 1.

We begin with a single grating, corresponding to one layer of this lattice. A plane wave of angular frequency ω and unit amplitude, is incident onto the grating with wave vector $(\alpha_0, -\chi_0)$ perpendicular to the axes of the cylinders, and wave number $k = \omega/c = (\alpha_0^2 + \chi_0^2)^{1/2}$, where c is the speed of light in vacuum. The grating generates various reflected and transmitted orders (channels) p that may be propagating or evanescent. The direction sines and cosines of the associated plane wave fields are given by

$$\sin\theta_p = \alpha_p/k, \quad \alpha_p = 2\pi p/d_x + \alpha_0, \tag{2}$$

$$\cos\theta_p = \chi_p/k, \quad \chi_p = \sqrt{k^2 - \alpha_p^2}, \tag{3}$$

with the χ_p being real for propagating orders and positive imaginary for evanescent orders.

For each grating, and for each possible incidence channel, we now introduce vectors of amplitude reflection and transmission coefficients that constitute the columns of the reflection and transmission *scattering matrices* that characterize the diffraction properties of the structure. In the case of our theory for a cylinder grating [15], the phase origin of amplitudes is taken to lie on a line through the centers of the cylinders. In general, four scattering matrices are required — $\mathbf{R}^{(0)}$ and $\mathbf{T}^{(0)}$ representing reflection and transmission scattering corresponding to incidence from above (i.e., from $y > 0$ in Fig. 1), and $\mathbf{R}'^{(0)}$ and $\mathbf{T}'^{(0)}$ being the corresponding quantities for incidence from below the grating (i.e., from $y < 0$). The (p_1, p_2) element of matrix $\mathbf{T}^{(0)}$, for example, represents the transmitted amplitude in channel p_1 corresponding to unit incidence amplitude from above in channel p_2. The matrices defined in this way, of course, depend on the incidence angle and frequency through the quantities k and α_0.

In the present paper we assume that the matrices $\mathbf{R}^{(0)}$, $\mathbf{T}^{(0)}$, $\mathbf{R}'^{(0)}$, and $\mathbf{T}'^{(0)}$ are known from the outset for all gratings. These matrices are of infinite dimension and must be truncated for computational purposes, keeping sufficient plane wave orders to ensure that the solution is well characterized and stable. For the cylinder gratings that we consider here, this can be done using multipole methods discussed earlier [15,16]. However, scattering matrices for these and other grating structures may be generated using integral equation techniques, differential methods as well as modal methods. Indeed, for a y-symmetric structure such as the simple cylinder grating we have $\mathbf{R}^{(0)} = \mathbf{R}'^{(0)}$ and $\mathbf{T}^{(0)} = \mathbf{T}'^{(0)}$. Nevertheless, while the theory developed here does not depend on the details of the geometry in general, there are a number of elegant simplifications that follow for specific symmetries.

Assuming no interpenetration of layers, the field at the edge of the layer interface ($y = \pm d_y/2$) may be expanded in terms of plane waves. From here on, the phase origins of the fields above and below the grating are taken to lie respectively on the centers of the upper and lower edges of the parallelogram unit cell (see Fig. 1) at points $P_j = (x_j, y_j) = \pm(s_x/2, d_y/2)$, $j = 1,2$. Fields above and below the grating ($j = 1$ and $j = 2$, respectively) are then expanded in the form

$$V^{(j)}(\mathbf{r}) = \sum_{p=-\infty}^{\infty} \chi_p^{-1/2} [f_p^{(j)-} e^{-i\chi_p(y-y_j)} + f_p^{(j)+} e^{i\chi_p(y-y_j)}] \exp[i\alpha_p(x-x_j)]. \tag{4}$$

In Eq. (4), the wave amplitudes are denoted by $f_p^{(j)\pm}$, with the prefactors $\chi_p^{-1/2}$ introduced so as to normalize energy quantities as the square modulus of the corresponding complex amplitude [15,16]. If the incident wave is $E_\parallel$ polarized (the electric field is perpendicular to the plane of incidence), V denotes the z component of the electric field E_z, while for a $H_\parallel$ polarized wave (the electric field is parallel to the plane of incidence) V denotes H_z. Note that the plane of incidence is defined by the direction of incident radiation and the normal to the grating plane. Here, we consider only the case of in-plane incidence so that the plane of incidence is the x-y plane, perpendicular to the axes of the cylinders.

It is clear that the $f_p^{(j)\pm}$ must be related to one another through the reflection and transmission scattering matrices of the grating. However, as the field phase origins of each individual grating do not coincide, in general, with the phase origins P_1 and P_2 it is necessary to transform the basic scattering matrices ($\mathbf{R}^{(0)}$, $\mathbf{T}^{(0)}$, etc.). If the basic scattering matrices have their phase origin at the origin of coordinates (as is the case for the simple cylinder grating), it is straightforward to show that the transformed scattering matrices with phase origins at points P_1 and P_2 are given by

$$\begin{bmatrix} \mathbf{T} & \mathbf{R}' \\ \mathbf{R} & \mathbf{T}' \end{bmatrix} = \mathcal{Q}\mathcal{P} \begin{bmatrix} \mathbf{T}^{(0)} & \mathbf{R}'^{(0)} \\ \mathbf{R}^{(0)} & \mathbf{T}'^{(0)} \end{bmatrix} \mathcal{P}\mathcal{Q}, \tag{5}$$

where

$$\mathcal{Q}=\begin{bmatrix}\mathbf{Q^{-1}} & \mathbf{0}\\ \mathbf{0} & \mathbf{Q}\end{bmatrix},\quad \mathcal{P}=\begin{bmatrix}\mathbf{P} & \mathbf{0}\\ \mathbf{0} & \mathbf{P}\end{bmatrix},$$

0 represents the zero matrix, and

$$\mathbf{Q}=\mathrm{diag}[e^{i\alpha_p s_x/2}],\quad \mathbf{P}=\mathrm{diag}[e^{i\chi_p d_y/2}]. \tag{6}$$

Denoting by $\mathbf{f}_j^{\pm}$ $(j=1,2)$ a column vector with elements $f_p^{(j)\pm}$, we can write the scattering of the incoming fields, $\mathbf{f}_1^-$ and $\mathbf{f}_2^+$, from the grating in the matrix form

$$\begin{bmatrix}\mathbf{f}_2^-\\ \mathbf{f}_1^+\end{bmatrix}=\begin{bmatrix}\mathbf{T} & \mathbf{R}'\\ \mathbf{R} & \mathbf{T}'\end{bmatrix}\begin{bmatrix}\mathbf{f}_1^-\\ \mathbf{f}_2^+\end{bmatrix}. \tag{7}$$

B. Bloch condition

Returning to the array structure, we now search for quasiperiodic solutions satisfying Bloch's theorem

$$u(\mathbf{r}+\mathbf{l}_{mn})=e^{i\mathbf{k}_0\cdot\mathbf{l}_{mn}}u(\mathbf{r}), \tag{8}$$

where u is any field quantity, and $\mathbf{k}_0=\alpha_0\hat{\mathbf{x}}+\beta_0\hat{\mathbf{y}}$ denotes the Bloch vector. The quasiperiodicity condition (4), in the x direction, is consistent with the family of plane wave fields that have direction sines α_p/k. In contrast, there is no such constraint for the quasiperiodicity in the y direction, and, in the procedures discussed below, β_0 is thus treated as an eigenvalue. Quasiperiodicity in the y direction is characterized by

$$\mathbf{f}_2^-=\mu\mathbf{f}_1^-,\quad \mathbf{f}_2^+=\mu\mathbf{f}_1^+, \tag{9}$$

where

$$\mu=\exp(-i\mathbf{k}_0\cdot\mathbf{e}_2). \tag{10}$$

Combining Eq. (9) with Eq. (7), we obtain

$$\mathbf{WF}=\mathbf{0}, \tag{11}$$

where

$$\mathbf{W}=\begin{bmatrix}\mathbf{T}-\mu\mathbf{I} & \mathbf{R}'\\ \mathbf{R} & \mathbf{T}'-\mu^{-1}\mathbf{I}\end{bmatrix},\quad \mathbf{F}=\begin{bmatrix}\mathbf{f}_1^-\\ \mathbf{f}_2^+\end{bmatrix}. \tag{12}$$

We now consider the structure of the eigenvalue equation (12). For computational purposes, all infinite dimensional matrices are truncated and so

$$P(\mu)=\det\mathbf{W}=0 \tag{13}$$

is a polynomial with terms in μ and μ^{-1}. For lattices for which $s_x=0$, i.e., for rectangular lattices of vertically symmetric scattering elements that are also symmetric with respect to $y=0$, it can be shown that $\mathbf{T}'=\mathbf{T}$ and $\mathbf{R}'=\mathbf{R}$, and thus $P(\mu)=P(1/\mu)$. Accordingly, for each root μ of Eq. (12) there must be a root μ^{-1}, with such a pair corresponding to forward and backward propagation through the lattice.

C. Symmetric lattices

We will return to a discussion of the distribution of the eigenvalues in Sec. II E but note here that the existence of such relations for symmetric structures enables a factorization of the eigenvalue equation, yielding an eigenvalue problem of half the dimension of the general form to be introduced in Sec. II D. Aside from being more computationally compact, they are also more stable numerically, avoiding theinversion of matrices whose conditioning may be problematic.

We commence with y-symmetric structures composed of y-symmetric gratings arranged in a rectangular array. Noting that $\mathbf{R}=\mathbf{R}'$ and $\mathbf{T}=\mathbf{T}'$, we apply the unitary transformation

$$\mathcal{I}=\frac{1}{\sqrt{2}}\begin{bmatrix}\mathbf{I} & \mathbf{I}\\ -\mathbf{I} & \mathbf{I}\end{bmatrix} \tag{14}$$

to Eq. (11) to derive

$$\mathbf{W}'\begin{bmatrix}\mathbf{g}_1\\ \mathbf{g}_2\end{bmatrix}=\begin{bmatrix}\mathbf{0}\\ \mathbf{0}\end{bmatrix}, \tag{15}$$

where

$$\mathbf{W}'=\mathcal{I}\mathbf{W}\mathcal{I}^T=\begin{bmatrix}\mathbf{T}+\mathbf{R}-c\mathbf{I} & is\mathbf{I}\\ is\mathbf{I} & \mathbf{T}-\mathbf{R}-c\mathbf{I}\end{bmatrix}, \tag{16}$$

$$\begin{bmatrix}\mathbf{g}_1\\ \mathbf{g}_2\end{bmatrix}=\mathcal{I}\begin{bmatrix}\mathbf{f}_1^-\\ \mathbf{f}_2^+\end{bmatrix}=\frac{1}{\sqrt{2}}\begin{bmatrix}\mathbf{f}_1^-+\mathbf{f}_2^+\\ -\mathbf{f}_1^-+\mathbf{f}_2^+\end{bmatrix}, \tag{17}$$

with $c=(\mu+\mu^{-1})/2=\cos\gamma$, $s=(\mu-\mu^{-1})/(2i)=\sin\gamma$.

From Eq. (15) we have a linear system that can be converted into a pair of equivalent eigenvalue equations

$$\mathcal{S}_i^{-1}\mathbf{T}\mathbf{g}_i=\frac{1}{2c}\mathbf{g}_i\quad (i=1,2), \tag{18}$$

where

$$\mathcal{S}_1=\mathbf{I}+(\mathbf{T}-\mathbf{R})(\mathbf{T}+\mathbf{R}), \tag{19}$$

$$\mathcal{S}_2=\mathbf{I}+(\mathbf{T}+\mathbf{R})(\mathbf{T}-\mathbf{R}). \tag{20}$$

The eigenvalue equation (18) is highly stable and computationally tractable. Since the eigenvalues occur in the form $2c=\mu+1/\mu$, the eigenvalues μ and $1/\mu$ must be paired; that is, if μ is an eigenvalue, then so is $1/\mu$. The occurrence of $1/(2c)$ in Eq. (18) implies that the eigenvalues are generated with the real or propagating states ($|c|\leqslant 1$) occurring before the evanescent or nonpropagating states ($|c|>1$). Either of the problems (18) may be solved to generate c and either of $\mathbf{g}_1$ or $\mathbf{g}_2$, with the other vector of the pair being inferred from the system (15) and (16). From these, $\mathbf{f}_1^-$ and $\mathbf{f}_2^+$ are generated from an inversion of Eq. (17). As will become apparent below, the pairs of vectors $(\mathbf{f}_1^-,\mathbf{f}_1^+)$ (where $\mathbf{f}_1^+=\mu^{-1}\mathbf{f}_2^-$) are very significant and may be used to form a reflection scattering matrix for a semi-infinite medium of inclusions.

For y-symmetric structures with $s_x = d_x/2$, the grating layers interleave one another uniformly, as in a hexagonal lattice. With this value of s_x, then $\mathbf{Q} = \exp(i\alpha_0 d_x/4)\mathbf{Q}_0$, where $\mathbf{Q}_0 = \mathrm{diag}\exp(ip\pi/2)$ and it follows that the eigenvalue problem of Eqs. (11) and (12) may be transformed to the form

$$\tilde{\mathbf{W}}\tilde{\mathbf{F}} = \mathbf{0}, \quad \text{where} \quad \tilde{\mathbf{W}} = \begin{bmatrix} \tilde{\mathbf{T}} - \tilde{\mu}\mathbf{I} & \tilde{\mathbf{R}} \\ \tilde{\mathbf{R}} & \tilde{\mathbf{T}} - \tilde{\mu}^{-1}\mathbf{I} \end{bmatrix}, \tag{21}$$

with

$$\tilde{\mathbf{T}} = \mathbf{Q}_0^{-1}\mathbf{P}\mathbf{T}^{(0)}\mathbf{P}\mathbf{Q}_0^{-1}, \tag{22}$$

$$\tilde{\mathbf{R}} = \mathbf{Q}_0^{-1}\mathbf{P}\mathbf{R}^{(0)}\mathbf{P}\mathbf{Q}_0^{-1}, \tag{23}$$

$$\tilde{\mu} = \mu \exp(i\alpha_0 d_x/2). \tag{24}$$

The form of the eigenvalue equation (21) is identical to that for the rectangular array and is thus amenable to the same transformation used to factor (18). The only essential difference is the replacement of μ by $\tilde{\mu}$ leading to deduction that the eigenvalues $\tilde{\mu}$ and $1/\tilde{\mu}$ are paired. This is illustrated later in Sec. II E.

We finally observe that the above pairing relations are derived through algebraic manipulation of the eigenvalue equations, relying solely on the y symmetry of the grating and the rectangular and centered rectangular symmetries of the lattice. Since nothing has been assumed about the material properties of gratings, the pairing relations are purely structural in their origin and hold for both lossless and absorbing gratings.

D. General treatment

The general treatment of the eigenvalue problem must be used in the absence of any symmetry and requires the formulation in terms of the $\mathcal{T}$ matrix [11,17,18]. Returning to Eq. (7), the eigenvalue problem may be cast in the form

$$\begin{bmatrix} \mathbf{f}_2^- \\ \mathbf{f}_2^+ \end{bmatrix} = \mathcal{T}\begin{bmatrix} \mathbf{f}_1^- \\ \mathbf{f}_1^+ \end{bmatrix}, \tag{25}$$

where the scattering matrix $\mathcal{T}$ is given by

$$\mathcal{T} = \begin{bmatrix} \mathbf{T} - \mathbf{R}'\mathbf{T}'^{-1}\mathbf{R} & \mathbf{R}'\mathbf{T}'^{-1} \\ -\mathbf{T}'^{-1}\mathbf{R} & \mathbf{T}'^{-1} \end{bmatrix} \tag{26}$$

$$= \begin{bmatrix} \mathbf{T} & \mathbf{0} \\ \mathbf{0} & \mathbf{I} \end{bmatrix}\begin{bmatrix} \mathbf{I} - \mathbf{A}\mathbf{B} & \mathbf{A} \\ -\mathbf{B} & \mathbf{I} \end{bmatrix}\begin{bmatrix} \mathbf{I} & \mathbf{0} \\ \mathbf{0} & \mathbf{T}'^{-1} \end{bmatrix}, \tag{27}$$

where

$$\mathbf{A} = \mathbf{T}^{-1}\mathbf{R}', \quad \mathbf{B} = \mathbf{T}'^{-1}\mathbf{R}. \tag{28}$$

We note that the form in Eq. (27) is derived by factorizing the matrix in Eq. (26). Of significance in the back propagation problem is the ready construction of the matrix $\mathcal{T}^{-1}$, obtained by observing for any **A** and **B** that

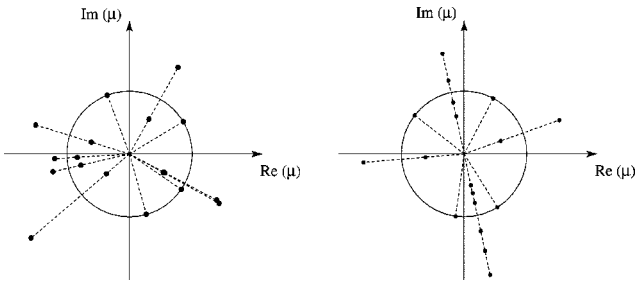

FIG. 2. Eigenvalue distribution for an arbitrary, nonsymmetric lattice (a) and for a hexagonal lattice (b). The scattering matrix data corresponds to a unit period grating $d_x = 1$ of cylinder voids of radius $a = 0.3921$ and refractive index $\nu = 0.8636$ arranged in a unit cell characterized by $s_x = 0.3420 d_x$, $d_y = 0.8660 d_x$ (nonsymmetric lattice), and $s_x = d_x/2$, $d_y = d_x\sqrt{3}/2$ (hexagonal lattice). Here, $k = 7.946\,56$ and $\alpha_0 = 2.717\,88$. For the hexagonal lattice the primary ray along which many of the eigenvalues are clustered is $\theta = -\alpha_0 d_x/2 = -1.358\,94$.

$$\begin{bmatrix} \mathbf{I} - \mathbf{A}\mathbf{B} & \mathbf{A} \\ -\mathbf{B} & \mathbf{I} \end{bmatrix}^{-1} = \begin{bmatrix} \mathbf{I} & -\mathbf{A} \\ \mathbf{B} & \mathbf{I} - \mathbf{B}\mathbf{A} \end{bmatrix}, \tag{29}$$

thereby yielding

$$\mathcal{T}^{-1} = \begin{bmatrix} \mathbf{T}^{-1} & -\mathbf{T}^{-1}\mathbf{R}' \\ \mathbf{R}\mathbf{T}^{-1} & \mathbf{T}' - \mathbf{R}\mathbf{T}^{-1}\mathbf{R}' \end{bmatrix}. \tag{30}$$

The Bloch factors μ are the eigenvalues of Eq. (25) and thus

$$\mathcal{T}\begin{bmatrix} \mathbf{f}_1^- \\ \mathbf{f}_1^+ \end{bmatrix} = \mu\begin{bmatrix} \mathbf{f}_1^- \\ \mathbf{f}_1^+ \end{bmatrix} \tag{31}$$

from which the μ and $\mathbf{f}_j^{\pm}$ can be obtained using standard techniques. Some care is required in the computation of $\mathbf{T}^{-1}$ and $\mathbf{T}'^{-1}$ and, for structures that exhibit particular symmetries, the forms of the preceding section are numerically more robust.

In any numerical implementation, the plane wave series are truncated to contain N_p terms and the matrix $\mathcal{T}$ is therefore of dimension $2N_p$, and consequently has $2N_p$ eigenvalues. In what follows, we assume that $\mathcal{T}$ is not defective and thus possesses a complete basis of linearly independent eigenvectors. While problems in the accuracy of the extreme (very large and very small) eigenvalues can arise, in practice only a truncated set of the eigenvalues μ in the vicinity of the unit circle are of real significance (see, in particular, Sec. III). Our experience has been that the most significant eigenvalues (i.e., those having the least absolute values of $c = (\mu + \mu^{-1})/2$) are stable with increasing matrix size (i.e., increasing N_p).

E. Classification of the eigensystem

The pairing of eigenvalues can occur irrespective of lattice symmetry, again partitioning the set of eigenvalues into forward and backward propagating states. Figure 2(a) shows the eigenvalue distribution for an arbitrary, lossless lattice (whose constituent element is the y-symmetric cylinder grat-

ing), with rays drawn from the origin to each eigenvalue μ in the complex plane. The plot region has been scaled radially according to $r=|\mu|^{0.04}$ (with r denoting the distance of the plotted point from the origin) to compress the dynamic range of the data. On each ray, there is an even number of eigenvalues (at least one pair) and thus we deduce the pairing rule that if μ is an eigenvalue then so is $\overline{\mu}^{-1}$, where the superposed bar denotes the complex conjugate. While this property has been demonstrated for lossless structures in all of our computational work, an analytic proof of its existence has thus far eluded us. This property fails to exist, however, for absorbing gratings and possibly points to an application of time reversibility in its derivation for lossless structures.

Figure 2(b) shows the eigenvalue distribution for a lossless hexagonal lattice. The previous $(\mu,\overline{\mu}^{-1})$ pairing is again evident, as is the $(\tilde{\mu},\tilde{\mu}^{-1})$ pairing derived in Sec. II C. Again, we note that for lossy materials the former pairing fails while the latter pairing, whose origin is purely structural, is preserved. As $\tilde{\mu}=\mu\exp(i\alpha_0 d/2)$, then for lossless materials $\tilde{\mu}$ is associated with both $\overline{\tilde{\mu}}^{-1}$ and $\tilde{\mu}^{-1}$. Hence, for this symmetry, $\tilde{\mu}$ is also paired with $\overline{\tilde{\mu}}$, implying that the $\tilde{\mu}$ must be real or occur in complex conjugate pairs. This is evident in Fig. 2(b), recalling that the distribution of the μ differs from that of $\tilde{\mu}$ by a rotation of $\theta=-\alpha_0 d/2$. Precisely the same structure occurs for lattices exhibiting rectangular symmetry, this time with a principal axis of $\theta=0$.

We next partition the set of eigenvalues and eigenvectors into forward and backward propagating states. In the presence of loss, eigenvalues have either $|\mu|<1$ or $|\mu|>1$, while for lossless structures some eigenvalues may have $|\mu|=1$. Now, designating the form of the eigenvector corresponding to an eigenvalue μ_i to be $[\mathbf{f}_i^{-T}\mathbf{f}_i^{+T}]^T$ (suppressing the previous subscript for convenience), the vector $\mathbf{f}_i^-$ denotes the ''eigenincidence'' into the layer from above, and $\mathbf{f}_i^+$ the corresponding ''eigenreflection.'' The pairing of eigenvalues above leads to a natural partitioning of the eigenstates. The evanescent states are characterized by $|\mu|\neq 1$ and so for each state such that $|\mu|<1$ there is one for which $|\mu|>1$. The decay of the field in the forward propagation problem is thus mirrored by the associated eigenvalue that represents decay in the back propagation problem.

Propagating states have magnitude $|\mu|=1$ and are again paired, representing forward and backward propagation. Unlike the evanescent states, that can be differentiated according to whether their magnitudes are greater than or less than unity, the classification of propagating states can be determined only from a consideration of the direction of energy flow characterized by the group velocity (see the Appendix) that is proportional to $\mathcal{E}_F/(k\mathcal{E}_D)$, where $\mathcal{E}_F$ denotes the downward energy flux and $\mathcal{E}_D$ is the energy density per unit cell. The flux $\mathcal{E}_F$ associated with a particular eigenstate is given by

$$\mathcal{E}_F=\sum_{p\in\Omega_r}(|f_p^-|^2-|f_p^+|^2)-2\,\mathrm{Im}\sum_{p\notin\Omega_r}f_p^-\overline{f_p^+}\,, \qquad (32)$$

where Ω_r denotes the set of propagating plane wave propagating orders. This form of $\mathcal{E}_F$ is derived from an application of Green's theorem [16] to the function V (4). Since $\mathcal{E}_D$ is purely positive, the direction of energy flow is determined entirely by the sign of $\mathcal{E}_F$.

TABLE I. Properties of the 18 most significant modes for the data corresponding to a hexagonal lattice displayed in Fig. 2(b). Columns 2 and 3 give the modulus and argument of the eigenvalues $\tilde{\mu}=\mu\exp(i\alpha_0 d/2)$, while column 4, only the sign of which is important, gives the energy flux (32).

n	$\lvert\tilde{\mu}\rvert$	$\arg(\tilde{\mu})/\pi$	$\mathcal{E}_F$
1	2.250×10^{7}	0.0000	0.0000
2	2.117×10^{5}	1.0000	0.0000
3	1.491×10^{5}	−0.5401	0.0000
4	1.491×10^{5}	0.5401	0.0000
5	8.650×10^{4}	0.0000	0.0000
6	2.885×10^{2}	0.0000	0.0000
7	8.856×10^{2}	1.0000	0.0000
8	1.000×10^{0}	0.1105	−0.9783
9	1.000×10^{0}	−0.7785	−0.9900
10	1.000×10^{0}	0.7785	0.9900
11	1.000×10^{0}	−0.1105	0.9783
12	1.129×10^{-2}	1.0000	0.0000
13	3.466×10^{-3}	0.0000	0.0000
14	1.1561×10^{-5}	0.0000	0.0000
15	6.7068×10^{-6}	0.5410	0.0000
16	6.7068×10^{-6}	−0.5410	0.0000
17	4.7237×10^{-6}	1.0000	0.0000
18	4.4435×10^{-8}	0.0000	0.0000

When $\mathcal{E}_F$ is positive there is a net flow of energy downward (i.e., into the structure), which we associate with forward propagation. Conversely, when $\mathcal{E}_F$ is negative, the net flow of energy is upwards away from the structure, and this is associated with backward propagation. This relationship is perhaps seen most clearly in the simple case of a y-symmetric grating embedded in a rectangular lattice for which $\mathbf{R}=\mathbf{R}'$ and $\mathbf{T}=\mathbf{T}'$. Here, the eigenvectors corresponding to μ and μ^{-1} are

$$\begin{bmatrix}\mathbf{f}^-\\ \mathbf{f}^+\end{bmatrix},\quad \begin{bmatrix}\mathbf{f}^+\\ \mathbf{f}^-\end{bmatrix}, \qquad (33)$$

respectively—a result that follows readily from the structure of the original system of equations (11) and (12). The change from forward to backward propagation involves the transposition of μ and μ^{-1}, which in turn reverses the roles of $\mathbf{f}^+$ and $\mathbf{f}^-$, thus reversing the direction of energy flow.

Table I displays the eigenvalues of $\boldsymbol{\mathcal{T}}$ that was used to generate Fig. 2(b). The data (see Figs. 7 and 8) correspond to a hexagonal lattice of cylindrical voids in an arbitrary incidence configuration, with the most significant $N=18$ eigenvalues shown. Eigenvalues 1–9 and 10–18, respectively correspond to the backward and forward travelling states. Eigenstates 8–11 are propagating states, with the direction of propagation being determined by the sign of the energy flux

(column 3)—with positive fluxes indicating downward, or forward, propagation. The remaining states are evanescent and carry no energy.

F. Application to band diagrams

We now apply the above method to the calculation of band structures, commencing with the procedure for the simple case of a rectangular lattice of sides d_1 and d_2. The primitive cell is then spanned by $\mathbf{e}_1=(d_1,0)$ and $\mathbf{e}_2=(0,d_2)$, and the associated primitive cell in reciprocal space is spanned by $\mathbf{u}_1=2\pi(d_1^{-1},0)$ and $\mathbf{u}_2=2\pi(0,d_2^{-1})$. Any point $\mathbf{k}_0=(\alpha_0,\beta_0)$ (in Cartesian coordinates) in reciprocal space may then be written

$$\mathbf{k}_0=\xi_1\mathbf{u}_1+\xi_2\mathbf{u}_2. \tag{34}$$

Consider now a diffraction problem for a single constituent grating of this lattice, the plane of which is parallel to $\mathbf{e}_1$ (and $\hat{z}$) and has period d_1. We consider an incident plane wave (possibly evanescent) of fixed frequency and incident angle θ_0, and observe that the phase change of the field over one period in the plane of the grating is $\mathbf{k}_0\cdot\mathbf{e}_1=kd_1\sin\theta_0=2\pi\xi_1$. Using the methods of Secs. II C and II D, we generate scattering matrices and then solve the eigenvalue problem to yield eigenvalues $\mu=\exp(-i\mathbf{k}_0\cdot\mathbf{e}_2)$ [see Eq. (10)]. From Sec. II B we recall that ξ_2 is an eigenvalue of the problem, the value of which is $\xi_2=-\arg\mu/(2\pi)$, since $\mathbf{k}_0\cdot\mathbf{e}_2=2\pi\xi_2$. Each propagating solution ($\xi_2\in[-1/2,1/2]$) found in this way lies on the line of fixed ξ_1 in the primitive cell of the reciprocal lattice. We thus generate the band structure in the line defined by fixed ω and ξ_1. The complete band structure is generated by varying ω and ξ_1 (or θ_0) [11]. We note, in contrast, that plane wave methods generate the band structure in a different order with fixed ξ_1 and ξ_2 defining an eigenproblem in which ω is the eigenvalue.

Of course the band structure can also be generated by considering diffraction by a constituent grating of period d_2 that is parallel to $\mathbf{e}_2$. The only difference is that we now generate the band structure from a line of constant ω and ξ_2. In fact, we can use any constituent grating that is parallel to the plane specified by $\hat{z}$ and $h_1\mathbf{e}_1+h_2\mathbf{e}_2$ (where $[h_1h_2]$ are the Miller indices) to generate the band structure on lines of constant ω, orthogonal to this plane. In order to deal with this general case, and with the most general crystal lattice, it is necessary to introduce a general framework that can cope with nonorthogonal basis vectors and arbitrary sections through the array.

For a general lattice, we introduce general basis vectors $\mathbf{e}_1$ and $\mathbf{e}_2$ for the direct lattice, and basis vectors $\mathbf{u}_1$ and $\mathbf{u}_2$ for the reciprocal lattice satisfying

$$\mathbf{u}_1\cdot\mathbf{e}_1=2\pi,\quad \mathbf{u}_1\cdot\mathbf{e}_2=0;$$
$$\mathbf{u}_2\cdot\mathbf{e}_1=0,\quad \mathbf{u}_2\cdot\mathbf{e}_2=2\pi. \tag{35}$$

As above, we take the lattice to be composed of constituent gratings parallel to both $\mathbf{e}_1$ and $\mathbf{e}_2$. It is convenient to formulate the method in terms of "formal" parameters $\tilde{\mathbf{e}}_1$ and $\tilde{\mathbf{e}}_2$,

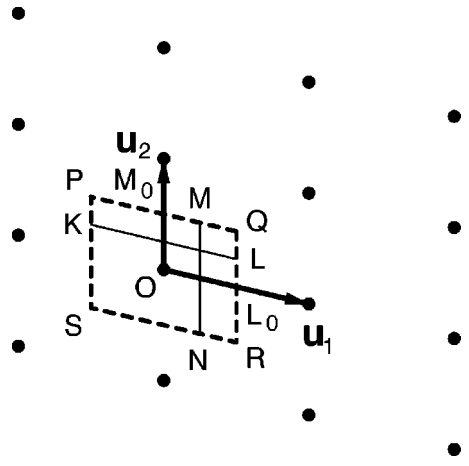

FIG. 3. The unit cell and fundamental translation vectors for the reciprocal of an arbitrary lattice.

into which we may substitute the actual vectors $\mathbf{e}_1$ and $\mathbf{e}_2$, or some linear combination, as required for a particular instance. In what follows, the formal parameters are uniformly denoted by the tilde nomenclature.

The grating code, i.e., the implementation of the diffraction theory for a single grating, may be regarded as an algorithm $\mathcal{A}=\mathcal{A}(\omega,\tilde{k}_{0g},\tilde{d})$ that computes scattering matrices of a single grating of period $\tilde{d}$ that is irradiated with a field whose component of the Bloch vector in the grating plane is $\tilde{k}_{0g}$. We formally take the plane of the grating to be aligned with $\tilde{\mathbf{e}}_1$ and to have period $\tilde{d}=\|\tilde{\mathbf{e}}_1\|$. The projection of the Bloch vector onto the plane of the grating is $\tilde{k}_{0g}=\mathrm{proj}_{\tilde{\mathbf{e}}_1}\mathbf{k}_0$ and the grating is periodically replicated with displacement $\tilde{\mathbf{e}}_2$ to form the lattice.

We must also introduce formal reciprocal lattice vectors $\tilde{\mathbf{u}}_1$ and $\tilde{\mathbf{u}}_2$ that satisfy relations identical to those in Eq. (35). Then, expanding the Bloch vector $\mathbf{k}_0$ in this basis, we write

$$\mathbf{k}_0=\tilde{\xi}_1\tilde{\mathbf{u}}_1+\tilde{\xi}_2\tilde{\mathbf{u}}_2. \tag{36}$$

We begin by regarding the array as the replication of a basic grating element $\mathcal{G}$ aligned with $\tilde{\mathbf{e}}_1=\mathbf{e}_2$, shifting each layer relative to its predecessor by $\tilde{\mathbf{e}}_2=-\mathbf{e}_1$. In reciprocal space, we have $\tilde{\mathbf{u}}_1=\mathbf{u}_2$ and $\tilde{\mathbf{u}}_2=-\mathbf{u}_1$. Consider now the line KL in reciprocal space (Fig. 3) which is parametrized by constant $\tilde{\xi}_1$ and varying $\tilde{\xi}_2\in[-1/2,1/2]$. From Eq. (35), it follows that $\mathbf{k}_0\cdot\tilde{\mathbf{e}}_1=2\pi\tilde{\xi}_1$, indicating that a one period step in the direction $\tilde{\mathbf{e}}_1$ advances the phase of the field in the grating plane by a constant $2\pi\tilde{\xi}_1$. To solve the required diffraction problem for grating $\mathcal{G}$, we specify $\tilde{k}_{0g}=\mathbf{k}_0\cdot\tilde{\mathbf{e}}_1/\tilde{d}_1$ with $\tilde{d}_1=\|\tilde{\mathbf{e}}_1\|$, and invoke the grating algorithm with $\mathcal{A}(\omega,2\pi\tilde{\xi}_1/\tilde{d}_1,\tilde{d}_1)$. We then compute the eigenvalues $\mu=\exp(-i\mathbf{k}_0\cdot\tilde{\mathbf{e}}_2)$ according to the methods of Secs. II C and II D, and from $\mathbf{k}_0\cdot\tilde{\mathbf{e}}_2=2\pi\tilde{\xi}_2$, we deduce $\tilde{\xi}_2=-\arg\mu/(2\pi)\in[-1/2,1/2]$. Finally, we reconstruct the eigenvalue $\mathbf{k}_0$ from

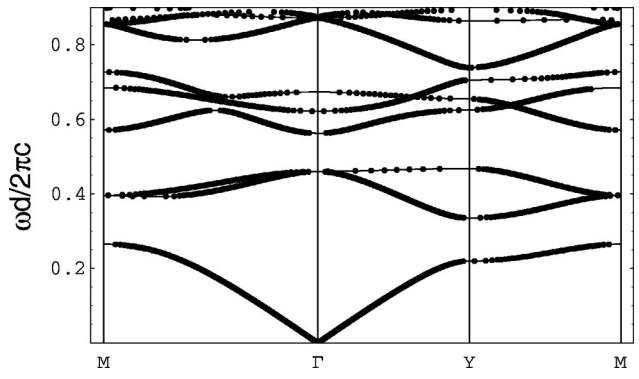

FIG. 4. The band diagram for a square symmetric lattice of dielectric cylinders of normalized radius $a/d=0.3$ and refractive index $\nu=3.0$, for $E_{\|}$ polarization. The continuous lines have been obtained from the Rayleigh multipole method, while the dots mark the eigenvalues β_0. The symbols on the abscissa represent the corners of the irreducible part of the first Brillouin zone (see Fig. 5).

$$\begin{bmatrix} \alpha_0 \\ \beta_0 \end{bmatrix} = \tilde{\mathbf{U}} \begin{bmatrix} \tilde{\xi}_1 \\ \tilde{\xi}_2 \end{bmatrix}, \tag{37}$$

where $\tilde{\mathbf{U}}$ is a matrix with columns $\tilde{\mathbf{u}}_1$ and $\tilde{\mathbf{u}}_2$.

In Fig. 3, the line OL_0 corresponds to $\tilde{\xi}_1=0$, i.e., normal incidence onto $\mathcal{G}$. The parallel edges of the primitive reciprocal cell, PQ and SR, respectively have $\tilde{\xi}_1=\pm 1/2$ for which $\mathbf{k}_0\cdot\tilde{\mathbf{e}}_1=\pm\pi$. In traditional grating terminology, these respectively correspond to Littrow mounts in the (-1)th and 1st orders—for which the plane wave orders ∓ 1 are respectively diffracted back along the path of the primary incident wave [19].

Similarly, the primitive cell may be scanned with lines parallel to $\tilde{\mathbf{u}}_1=\mathbf{u}_1$. This time, we consider incidence on the basic grating element $\mathcal{G}$ aligned with $\tilde{\mathbf{e}}_1=\mathbf{e}_1$ and replicated with spacing $\tilde{\mathbf{e}}_2=\mathbf{e}_2$. With these definitions, the above procedure carries through unaltered. We note that the scan line OM_0 corresponds to a normal incidence configuration onto a grating parallel to $\mathbf{e}_1$, while the edges RQ and SP correspond to first order Littrow configurations.

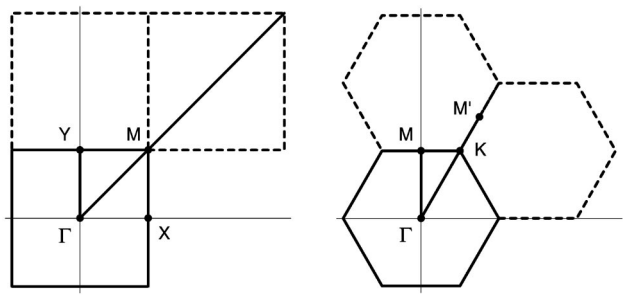

FIG. 5. The first Brillouin zone, and two of its replicates, for a square (left panel) and a hexagonal (right panel) array.

We now apply the method to the calculation of the band diagrams for two symmetric lattices. For the square array (Fig. 4), the diagram shows the dimensionless frequency $(\omega d/2\pi c)$ as a function of Bloch's vector $(\mathbf{k}_0)$ as the boundary ΓYMΓ of the irreducible part of the first Brillouin zone—the octant shown in the left panel of Fig. 5—is traversed. Table II shows the parametrization of the reciprocal lattice path and the direct lattice basis vectors $\tilde{\mathbf{e}}_1$, defining the grating plane, and $\tilde{\mathbf{e}}_2$ defining the replication displacement. The table shows that segments ΓY and MΓ are computed from the normal incidence properties of gratings of period d and $\sqrt{2}d$, while the segment YM requires a Littrow configuration for a grating of period d. The points in Fig. 4 have been calculated using this method, while the lines were calculated using the Rayleigh multipole theory applied to the whole array [20].

For the hexagonal array (Fig. 6), the irreducible part of the first Brillouin zone (Fig. 5) is parametrized in Table III. What is initially surprising is that the three segments can be handled using only two normal incidence calculations for gratings of periods d(ΓM) and $\sqrt{3}d$ (MK and KΓ). To see this, consider Table III, showing that on MK $\mathbf{k}_0\cdot\tilde{\mathbf{e}}_1=2\pi$—a second order Littrow configuration. In this case, we would be required to operate the grating code with $\tilde{k}_{0g}=2\pi/\tilde{d}_1$ leading to direction sines (of the plane wave orders) given by $\tilde{\alpha}_p/k$, where

TABLE II. Parametrized paths and basis gratings for each of the segments required to traverse the boundary of the first Brillouin zone for a square array of period d. The columns $\mathbf{k}_0$ and ''Range'' show the parametrization of the path and the range of the indicated parameter, while the vectors $\tilde{\mathbf{e}}_i$ show the basis vectors (in Cartesian coordinates) of the direct lattice used in the calculations. The columns $\tilde{d}_1/d$ and $\mathbf{k}_0\cdot\tilde{\mathbf{e}}_1$ show the normalized period and phase change along a period of the grating.

Path	$\mathbf{k}_0$	Range	$\tilde{\mathbf{e}}_1/d$	$\tilde{\mathbf{e}}_2/d$	$\tilde{d}_1/d$	$\mathbf{k}_0\cdot\tilde{\mathbf{e}}_1$
ΓY	$(0,k_{0y})$	$\left[0,\frac{\pi}{d}\right]$	(1,0)	(0,1)	1	0
YM	$\left(k_{0x},\frac{\pi}{d}\right)$	$\left[0,\frac{\pi}{d}\right]$	(0,1)	(−1,0)	1	π
MΓ	$k_0\left(\frac{1}{\sqrt{2}d},\frac{1}{\sqrt{2}d}\right)$	$\left[0,\frac{\pi\sqrt{2}}{d}\right]$	(−1,1)	(0,1)	$\sqrt{2}$	0

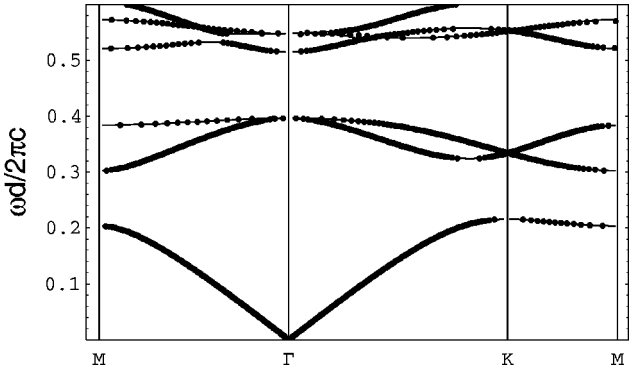

FIG. 6. The band diagram for a hexagonally symmetric lattice of dielectric cylinders of normalized radius $a/d=0.3$ and refractive index $\nu=3.6$, for $E_{\|}$ polarization. The continuous lines have been obtained from the Rayleigh multipole method, while the dots mark the eigenvalues β_0. The symbols on the abscissa represent the corners of the irreducible part of the first Brillouin zone (see Fig. 5).

$$\tilde{\alpha}_p=\tilde{\alpha}_0+2\pi p/\tilde{d}_1=2\pi(p+1)/\tilde{d}_1.$$

The list of direction sines $\{\tilde{\alpha}_p/k\}$ for this configuration is identical to that for normal incidence, except that the list is shifted by one place. The entries in the scattering matrices are similarly identical but shifted by one row and one column. The corresponding eigenproblems for normal incidence and the second order Littrow mount are thus equivalent, generating the same eigenvalues but with eigenvectors whose entries are displaced by one position. Thus, a single normal incidence calculation for a grating of period $\sqrt{3}d$ placed in a hexagonal array of spacing $d/2$ gives bands for both ΓK and MK. Due to the symmetry of the hexagonal array, $K\mathrm{M}'$, the extension of ΓK (see Fig. 5), is equivalent to KM. Note that, in the case of a square array, the extension of ΓM is not equivalent to any of the segments MY or ΓY. Consequently, to calculate the band diagram, we need three gratings for a square array but only two for a hexagonal array. In the case of a hexagonal array, the two sets of bands can be disentangled, since the arguments of the eigenvalues μ associated with ΓK are in the range $[-2\pi/3,0]$, while those associated with KM are in the range $[-\pi,-2\pi/3]$.

Once again, the photonic band diagram produced by this method (Fig. 6) is identical with the diagram obtained from the Rayleigh multipole theory for a hexagonal array [20]. In this case, however, in the application of the method for the segment ΓKM interpenetration occurs for radii $a/d>0.25$ and thus the application may not be strictly valid. However, as is evident from Fig. 6, the results are in excellent agreement with those obtained from multipole theory. In this regard, the insistence on noninterpenetration is a sufficient but not a necessary condition for the method. The issue is directly related to the Rayleigh controversy of diffraction grating theory [12] concerning the validity of plane wave representations for outgoing fields. The first insight into what, at the time (the 1960s), was a highly contentious problem came with the work of Petit and Cadilhac [21]. They considered an analytic continuation into the complex plane of the plane wave expansion of the outgoing field for a perfectly conducting, sinusoidal grating (Dirichlet boundary conditions) and demonstrated that the Rayleigh expansion converged provided that the groove depth was sufficiently shallow. The consideration of the Rayleigh hypothesis has since been further generalized [22–24] to show that use of the plane wave expansion is valid provided the series converges, with the crossover occurring at a singularity of the analytic continuation of the diffracted field. It is the location of the singularities that characterizes the necessary condition and, in our case, they depend on both the radius of the cylinders and their dielectric constant. While we have not closely investigated the nature of the necessary condition, nevertheless, we have observed the effects of layer interpenetration becoming evident more quickly with increasing refractive index of the cylinders.

III. SCATTERING IN FINITE STACKS

A. Formulation

Following the partitioning of the eigenstates into forward and backward propagation, it is natural to partition the eigenvalue equations (31) similarly. Recasting Eq. (31) for all i in matrix form we may write

$$\boldsymbol{\mathcal{T}}\tilde{\mathbf{F}}=\tilde{\mathbf{F}}\tilde{\Lambda}, \tag{38}$$

where

TABLE III. Parametrized paths and basis gratings for each of the segments required to traverse the boundary of the first Brillouin zone for a hexagonal array of period d. Other quantities are as defined in Table II.

Path	$\mathbf{k_0}$	Range	$\tilde{\mathbf{e}}_1/d$	$\tilde{\mathbf{e}}_2/d$	$\tilde{d}_1/d$	$\mathbf{k}_0\cdot\tilde{\mathbf{e}}_1$
ΓM	$(0,k_{0y})$	$\left[0,\frac{2\pi}{d\sqrt{3}}\right]$	(1,0)	$\left(\frac{1}{2},\frac{\sqrt{3}}{2}\right)$	1	0
MK	$\left(k_{0x},\frac{2\pi}{d\sqrt{3}}\right)$	$\left[0,\frac{2\pi}{3d}\right]$	$(0,\sqrt{3})$	$\left(-\frac{1}{2},\frac{\sqrt{3}}{2}\right)$	$\sqrt{3}$	2π
KΓ	$k_0\left(\frac{1}{2},\frac{\sqrt{3}}{2}\right)$	$\left[0,\frac{4\pi}{3d}\right]$	$\left(-\frac{3}{2},\frac{\sqrt{3}}{2}\right)$	$(-1,0)$	$\sqrt{3}$	0

$$\tilde{\mathbf{F}}=\begin{bmatrix}\mathbf{F}_- & \mathbf{F}'_- \\ \mathbf{F}_+ & \mathbf{F}'_+\end{bmatrix} \quad \text{and} \quad \tilde{\mathbf{\Lambda}}=\begin{bmatrix}\mathbf{\Lambda} & \mathbf{0} \\ \mathbf{0} & \mathbf{\Lambda}'\end{bmatrix}. \tag{39}$$

The left and right partitions of the block structured matrix $\tilde{\mathbf{F}}$ and the diagonal matrices $\mathbf{\Lambda}=\mathrm{diag}[\mu_i]$ and $\mathbf{\Lambda}'=\mathrm{diag}[\mu'_i]$ that constitute the left and right partitions of $\tilde{\mathbf{\Lambda}}$ respectively correspond to the forward and backward propagation problems.

The $\mathcal{T}$ matrix represents propagation across a single layer and, correspondingly,

$$\mathcal{T}^n=(\tilde{\mathbf{F}}\tilde{\mathbf{\Lambda}}\tilde{\mathbf{F}}^{-1})^n=\tilde{\mathbf{F}}\tilde{\mathbf{\Lambda}}^n\tilde{\mathbf{F}}^{-1} \tag{40}$$

denotes the propagation operator for a stack of n identical layers. Denoting

$$\tilde{\mathbf{F}}^{-1}\equiv\tilde{\mathbf{G}}\equiv\begin{bmatrix}\mathbf{G}_- & \mathbf{G}_+ \\ \mathbf{G}'_- & \mathbf{G}'_+\end{bmatrix} \tag{41}$$

and writing $\mathcal{T}^n$ in a form analogous to Eq. (25), we deduce

$$\begin{bmatrix}\mathbf{T}_n-\mathbf{R}'_n\mathbf{T}'^{-1}_n\mathbf{R}_n & \mathbf{R}'_n\mathbf{T}'^{-1}_n \\ -\mathbf{T}'^{-1}_n\mathbf{R}_n & \mathbf{T}'^{-1}_n\end{bmatrix}=\begin{bmatrix}\mathbf{F}_- & \mathbf{F}'_- \\ \mathbf{F}_+ & \mathbf{F}'_+\end{bmatrix}\begin{bmatrix}\mathbf{\Lambda}^n & \mathbf{0} \\ \mathbf{0} & \mathbf{\Lambda}'^n\end{bmatrix} \times\begin{bmatrix}\mathbf{G}_- & \mathbf{G}_+ \\ \mathbf{G}'_- & \mathbf{G}'_+\end{bmatrix}. \tag{42}$$

Similarly, from the form of the backward propagation operator $\mathcal{T}^{-1}$ (30) whose eigenvalues are the reciprocals of those for $\mathcal{T}$, we may form

$$\begin{bmatrix}\mathbf{T}^{-1}_n & -\mathbf{T}^{-1}_n\mathbf{R}'_n \\ \mathbf{R}_n\mathbf{T}^{-1}_n & \mathbf{T}'_n-\mathbf{R}_n\mathbf{T}^{-1}_n\mathbf{R}'_n\end{bmatrix}=\begin{bmatrix}\mathbf{F}_- & \mathbf{F}'_- \\ \mathbf{F}_+ & \mathbf{F}'_+\end{bmatrix}\begin{bmatrix}\mathbf{\Lambda}^{-n} & \mathbf{0} \\ \mathbf{0} & \mathbf{\Lambda}'^{-n}\end{bmatrix} \times\begin{bmatrix}\mathbf{G}_- & \mathbf{G}_+ \\ \mathbf{G}'_- & \mathbf{G}'_+\end{bmatrix}. \tag{43}$$

Expanding Eq. (43) and equating like terms we derive explicit expressions for the scattering matrices of the n layer structure in terms of those for a single layer. The computationally stable forms that we use in our calculations are

$$\mathbf{T}_n=\mathbf{G}^{-1}_-\mathbf{\Lambda}^n\mathbf{F}^{-1}_-[\mathbf{I}+\mathbf{F}'_-\mathbf{\Lambda}'^{-n}\mathbf{G}'_-\mathbf{G}^{-1}_-\mathbf{\Lambda}^n\mathbf{F}^{-1}_-]^{-1}, \tag{44}$$

$$\mathbf{R}_n=[\mathbf{I}+\mathbf{F}'_+\mathbf{\Lambda}'^{-n}\mathbf{G}'_-\mathbf{G}^{-1}_-\mathbf{\Lambda}^n\mathbf{F}^{-1}_+]\mathbf{F}_+\mathbf{F}^{-1}_- \times[\mathbf{I}+\mathbf{F}'_-\mathbf{\Lambda}'^{-n}\mathbf{G}'_-\mathbf{G}^{-1}_-\mathbf{\Lambda}^n\mathbf{F}^{-1}_-]^{-1}. \tag{45}$$

Similar expressions may be derived for $\mathbf{T}'_n$ and $\mathbf{R}'_n$ using Eq. (42).

Figure 7 displays the normal incidence reflection spectrum for an 88-layer stack that models a photonic crystal found in a living creature, the sea mouse [25,26]. The stack comprises a hexagonally packed array (of period $d=0.51$ μm) of hollow cylinders (of radius $a=0.2$ μm) filled with sea water of index $\nu_c=1.33$ in a matrix of chitin of refractive index $\nu_m=1.54$. The results have been calculated using Eq. (45) and are identical to those based on our earlier recurrence method [15]. The strong reflection around $\lambda=640$ nm gives the sea mouse its brilliant red iridescence [25,26] at normal incidence and is due to the partial band gap shown in Fig. 8. The band diagram has been computed using the theory of Sec. II C and II D and displays the band gap in complex $\mathbf{k}_0$ space, displaying the trajectory of the primary evanescent state crossing the gap.

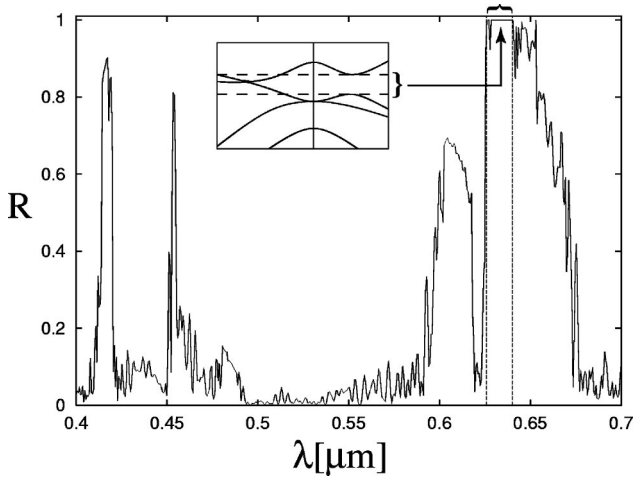

FIG. 7. Reflectance of a stack of 88 cylinder gratings (with $d_x=0.51$ μm), hexagonally packed, at normal incidence ($\alpha_0=0$). The cylinders are infinitely long, have a radius $a=0.2$ μm, and a refractive index $\nu_c=1.33$, and are embedded in a background with $\nu_m=1.54$. The vertical dashed lines correspond to the band gap in the photonic band diagram shown in the inset.

B. The matrix $\mathbf{R}_\infty$

It is natural now to examine the limit behavior with increasing stack depth ($n\to\infty$) to establish the reflection scattering matrix of a semi-infinite stack. The model must be formulated such that no wave can return from the bottom of the stack. While the evanescent terms are such that both $\mu^n,\mu'^{-n}\to 0$ as $n\to\infty$, it is necessary to suppress the reflection of propagating states, for which $|\mu|=|\mu'|=1$, from the bottom of the stack. This can be achieved conceptually by

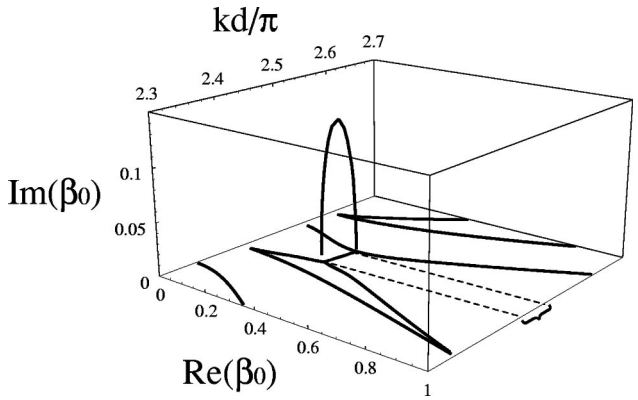

FIG. 8. Complex band diagram for the sea mouse spine, showing the gap states. Here, and in Fig. 7, the braces indicate the location of the partial band gap. Note that the $\mathrm{Im}(\beta_0)=0$ plane corresponds to the inset of Fig. 7.

introducing an arbitrarily small amount of loss, ensuring that the elements of both $\mathbf{\Lambda}'^{-1}$ and $\mathbf{\Lambda}$ have magnitudes less than unity and that powers of these matrices approach $\mathbf{0}$ with increasing n. Thus, from Eq. (45),

$$\mathbf{R}_\infty = \lim_{n\to\infty} \mathbf{R}_n = \mathbf{F}_+ \mathbf{F}_-^{-1}. \tag{46}$$

Correspondingly, a similar analysis based on Eq. (42) yields the reflection scattering matrix of the bulk crystal corresponding to propagation in the reverse direction,

$$\mathbf{R}'_\infty = \lim_{n\to\infty} \mathbf{R}'_n = \mathbf{F}'_- \mathbf{F}'^{-1}_+. \tag{47}$$

Two alternative forms for $\mathbf{R}_\infty$ and $\mathbf{R}'_\infty$,

$$\mathbf{R}_\infty = -\mathbf{G}'^{-1}_+ \mathbf{G}'_-, \quad \mathbf{R}'_\infty = -\mathbf{G}_-^{-1}\mathbf{G}_+, \tag{48}$$

may be established from Eqs. (42) and (43). The consistency of these forms with Eqs. (46) and (47) is assured by Eq. (41).

The computation of $\mathbf{R}_\infty$ using Eq. (46) can require some care as some of the spectral quantities can be difficult to obtain accurately for eigenvalues having extreme magnitudes. However, such problems may be overcome by truncating the column dimensions of $\mathbf{F}_+$ and $\mathbf{F}_-$ to accommodate only those most significant eigenstates—and those whose accuracy can be assured—and by computing the inverse of $\mathbf{F}_-$ using the generalized inverse through the singular value decomposition [27]. In this way, the product of the truncated matrices can be constructed as a series of projections that we have found to converge quite rapidly.

We complete this section with an alternative derivation of $\mathbf{R}_\infty$ and $\mathbf{R}'_\infty$ based directly on the defining eigensystem. In general, any field must be able to be written as a linear combination of eigenstates. Thus,

$$\begin{bmatrix} \mathbf{f}^- \\ \mathbf{f}^+ \end{bmatrix} = \sum_i \gamma_i \begin{bmatrix} \mathbf{f}_i^- \\ \mathbf{f}_i^+ \end{bmatrix} \tag{49}$$

for constants γ_i. It thus follows that

$$\mathbf{f}^- = \mathbf{F}_- \boldsymbol{\gamma}, \quad \mathbf{f}^+ = \mathbf{F}_+ \boldsymbol{\gamma}, \tag{50}$$

where the $\mathbf{F}_\pm$ are matrices with columns $\mathbf{f}_i^\pm$ and with $\boldsymbol{\gamma} = [\gamma_i]$. Eliminating $\boldsymbol{\gamma}$ from Eq. (50) yields

$$\mathbf{f}^+ = \mathbf{F}_+ \mathbf{F}_-^{-1} \mathbf{f}^-, \tag{51}$$

from which we infer the definition $\mathbf{R}_\infty = \mathbf{F}_+ \mathbf{F}_-^{-1}$.

C. Physical significance of the spectral quantities

To this point, the various spectral quantities associated with $\boldsymbol{\mathcal{T}}$ have been used in a relatively abstract manner. We now seek to attribute some physical significance to these quantities. We begin with $\boldsymbol{\mathcal{T}}^{-n}\tilde{\mathbf{F}} = \tilde{\mathbf{F}}\tilde{\mathbf{\Lambda}}^{-n}$ from Eq. (38), expanding the (1,1) partition to yield

$$\mathbf{T}_n^{-1}\mathbf{F}_- - \mathbf{T}_n^{-1}\mathbf{R}'_n\mathbf{F}_+ = \mathbf{F}_-\mathbf{\Lambda}^{-n}. \tag{52}$$

From this, it follows that

$$\mathbb{P}_n^- \overset{\text{def}}{=} (\mathbf{I} - \mathbf{R}'_n\mathbf{R}_\infty)^{-1}\mathbf{T}_n = \mathbf{F}_-\mathbf{\Lambda}^n\mathbf{F}_-^{-1}, \tag{53}$$

in which we have used the definition (46) of $\mathbf{R}_\infty$. This result holds for any n and is the spectral decomposition of the propagation matrix $\mathbb{P}_n$.

The significance of the result may be understood by considering a stack of n grating layers placed atop a stack of infinite depth, the reflection matrix of which is $\mathbf{R}_\infty$. The operator $\mathbb{P}_n$, when applied to a field $\mathbf{f}$ incident upon the top of the n-layer stack, generates the vector of amplitudes for the downward propagating field between the n-layer stack and the semiinfinite array below. In $\mathbb{P}_n$, the postmultiplied matrix $\mathbf{T}_n$ transmits the field through the n-layer structure while the matrix $(\mathbf{I}-\mathbf{R}'_n\mathbf{R}_\infty)^{-1}$ generates multiple reflections in the cavity by reflection of the down-going field off the array ($\mathbf{R}_\infty$) and of the up-going field reflecting off the n-layer structure from above ($\mathbf{R}'_n$). Similarly, the upward going field in the same interface is $\mathbb{P}_n^+\mathbf{f}$, where $\mathbb{P}_n^+ = \mathbf{R}_\infty\mathbb{P}_n^-$, whose spectral decomposition $\mathbb{P}_n^+ = \mathbf{F}_+\mathbf{\Lambda}^n\mathbf{F}_-^{-1}$. We finally note from Eq. (53) that for lossy gratings the eigenvalues must all have magnitude less than unity as absorption causes the fields to decay with increasing depth into the stack.

Accordingly, Eq. (53) indicates that the downward propagating field between the n-layer and the semi-infinite array can be understood as a superposition of Bloch functions of the structure, each of which is associated with its own eigenvalue or Bloch factor μ^n. Specifically, the matrix $\mathbf{F}_-^{-1}$ transforms a plane wave field to the natural Bloch basis, the diagonal matrix $\mathbf{\Lambda}^n$ scales each Bloch function by the associated Bloch factor, while the matrix $\mathbf{F}$ transforms the field back to the plane wave basis.

In a similar manner, we may also derive

$$(\mathbf{I}-\mathbf{R}\mathbf{R}'_\infty)^{-1}\mathbf{T}' = \mathbf{F}'_+\mathbf{\Lambda}'^{-1}\mathbf{F}'^{-1}_+, \tag{54}$$

$$\mathbf{T}'^{-1}(\mathbf{I}-\mathbf{R}\mathbf{R}_\infty^{-1}) = \mathbf{F}_+\mathbf{\Lambda}\mathbf{F}_+^{-1}, \tag{55}$$

$$\mathbf{T}^{-1}(\mathbf{I}-\mathbf{R}'\mathbf{R}'^{-1}_\infty) = \mathbf{F}'_-\mathbf{\Lambda}'^{-1}\mathbf{F}'^{-1}_-. \tag{56}$$

by expanding the various partitions of Eq. (43). The first of these, Eq. (54), is the single layer ($n=1$) analog of Eq. (53) except for propagation in the reverse direction. The physical meaning of Eqs. (55) and (56) is more difficult to deduce and, in fact, neither have real computational significance, except in the long wavelength asymptotics for which they provide a way of deducing $\mathbf{R}_\infty$ and $\mathbf{R}'_\infty$ directly. We have included them to show the matrices whose spectral decompositions define the outgoing fields $\mathbf{F}_+$ and $\mathbf{F}'_-$.

D. Asymptotic forms for deep arrays

The relationships of the Sec. III C, together with

$$\mathbf{F}_-\mathbf{G}_- = \mathbf{I} - \mathbf{R}'_\infty\mathbf{R}_\infty, \tag{57}$$

$$\mathbf{F}'_-\mathbf{G}'_- = -\mathbf{R}'_\infty\mathbf{R}_\infty(\mathbf{I}-\mathbf{R}'_\infty\mathbf{R}_\infty)^{-1}, \tag{58}$$

$$\mathbf{F}_+\mathbf{G}_- = \mathbf{R}_\infty(\mathbf{I}-\mathbf{R}'_\infty\mathbf{R}_\infty)^{-1} = -\mathbf{F}'_+\mathbf{G}'_-, \tag{59}$$

that follow from the definition of $\tilde{\mathbf{G}}$ (41), enable the transmission matrix (44) of an n-layer structure to be recast in the following, more physically significant form:

$$\mathbf{T}_n = (\mathbf{I}-\mathbf{R}'_\infty\mathbf{R}_\infty)(\mathbf{F}_-\mathbf{\Lambda}^{-n}\mathbf{F}_-^{-1} - \mathbf{F}'_-\mathbf{\Lambda}'^{-n}\mathbf{F}'^{-1}_-\mathbf{R}'_\infty\mathbf{R}_\infty)^{-1}. \tag{60}$$

This expression closely parallels the scalar transmission coefficient of a simple Fabry-Perot cavity [28]

$$T = \frac{1-\rho^2}{\exp(-i\varphi)-\rho^2\exp(i\varphi)}, \tag{61}$$

where ρ is the amplitude reflection coefficient of the mirrors and φ is the phase advance upon propagation through the cavity. Note the correspondence between the respective scalar and matrix quantities. In particular, observe the correspondence between the reflection quantities ρ^2 and $\mathbf{R}'_\infty\mathbf{R}_\infty$, and the phase factors $\exp(\mp i\varphi)$ and $\mathbf{\Lambda}^{-n}$ and $\mathbf{\Lambda}'^{-n}$. Note that for up-down symmetric structures, the matrices $\mathbf{\Lambda}$ and $\mathbf{\Lambda}'$ are inverses of one another. Equation (60) is therefore similar to the usual expression for the transmission of a Fabry-Perot filter, but generalizes it to include all the diffracted orders of the two ''mirrors.''

Finally, for the particular case of absorbing gratings, all eigenvalues of $\mathbf{\Lambda}$ have magnitudes less than 1 and all eigenvalues in $\mathbf{\Lambda}'$ have magnitudes greater than 1. Thus, $\mathbf{\Lambda}^n \to 0$ and $\mathbf{\Lambda}'^{-n} \to 0$, and for n sufficiently large we take these to be negligible. Using Eq. (25), Eq. (60) then reduces to

$$\begin{aligned}\mathbf{T}_n &\sim (\mathbf{I}-\mathbf{R}'_\infty\mathbf{R}_\infty)(\mathbf{F}_-\mathbf{\Lambda}^{-1}\mathbf{F}_-)^n \\ &\sim (\mathbf{I}-\mathbf{R}'_\infty\mathbf{R}_\infty)[(\mathbf{I}-\mathbf{R}'_\infty\mathbf{R}_\infty)^{-1}\mathbf{T}]^n,\end{aligned} \tag{62}$$

for large n.

IV. HOMOGENIZATION AND $\mathbf{R}_\infty$

As a demonstration of the significance of $\mathbf{R}_\infty$, we consider one- and two-dimensional photonic crystals in the long wavelength limit and demonstrate that $\mathbf{R}_\infty$ provides a useful mechanism for computing the effective dielectric constant of a homogenized medium.

We begin with a model of a one-dimensional photonic crystal in which the period cell consists of two uniform layers of refractive indices ν_1 and ν_2, of thicknesses c_1 and c_2, with $d_y = c_1 + c_2$. The Bloch factor, or propagation constant in the x direction, is $\alpha_0 = k\nu_1 \sin\theta_1 = k\nu_2 \sin\theta_2$, where θ_1 and θ_2 are the angles of the propagating rays in media 1 and 2. The corresponding propagation constants in the y direction are

$$\chi_i = \sqrt{k^2\nu_i^2 - \alpha_0^2}. \tag{63}$$

In this case, the reflection and transmission scattering matrices reduce to scalar form

$$R = \frac{\rho(1-e^{2i\chi_2 c_2})}{1-\rho^2 e^{2i\chi_2 c_2}} e^{i\chi_1 c_1}, \tag{64}$$

$$T = \frac{(1-\rho^2)e^{i\chi_2 c_2}}{1-\rho^2 e^{2i\chi_2 c_2}} e^{i\chi_1 c_1}, \tag{65}$$

where the multiplicative term $\exp(i\chi_1 c_1)$ is used to pad the layer of thickness c_2 with two background layers of index ν_1 and thickness $c_1/2$ to form a period layer of thickness d_y. In Eqs. (64) and (65), ρ denotes the interface reflection coefficient which, for $E_\parallel$ polarization, is $\rho = (\chi_1 - \chi_2)/(\chi_1 + \chi_2)$. After substituting R (64) and T (65) into the eigenvalue equation (11) we derive

$$\begin{bmatrix} T-\mu & \mu R \\ R & \mu T - 1 \end{bmatrix}\begin{bmatrix} f^- \\ f^+ \end{bmatrix} = \begin{bmatrix} 0 \\ 0 \end{bmatrix}, \tag{66}$$

which, after some manipulation, can be written in the Kronig-Penney form

$$\begin{aligned}&\cos(\chi_1 c_1)\cos(\chi_2 c_2) - \frac{1}{2}\left(\frac{\chi_1}{\chi_2} + \frac{\chi_2}{\chi_1}\right)\sin(\chi_1 c_1)\sin(\chi_2 c_2) \\ &\quad = \cos(\beta_0 d_y),\end{aligned} \tag{67}$$

where $\mu = \exp(i\beta d_y)$. The quasistatic limit of Eq. (67), in which we take small argument asymptotic expansions, yields

$$\chi_1^2 c_1 + \chi_2^2 c_2 = \beta_0^2 d_y, \tag{68}$$

reducing to

$$k^2\varepsilon_{\text{eff}} = \alpha_0^2 + \beta_0^2 \overset{\text{def}}{=} k_0^2, \tag{69}$$

where ε_{eff} is given by the Wiener formula [29] of electrostatics

$$\varepsilon_{\text{eff}} = \nu_1^2\frac{c_1}{d_y} + \nu_2^2\frac{c_2}{d_y}. \tag{70}$$

In the dispersion relation of Eq. (69), namely, $k\nu_{\text{eff}} = k_0$, $\mathbf{k}_{0,\perp} = (\alpha_0, \beta_0)$ is the projection of the crystal momentum onto the x-y plane and $\nu_{\text{eff}} = \sqrt{\varepsilon_{\text{eff}}}$. In keeping with the definition (63) of the propagation constants χ_i, it is natural to introduce the constant $\chi_\infty = \sqrt{k^2\varepsilon_{\text{eff}} - \alpha_0^2}$ corresponding to propagation in an unbounded medium of effective permittivity ε_{eff} and from Eq. (69) it is clear that $\beta_0 = \chi_\infty$.

The null vectors of the eigenequation then enable us to construct the reflection coefficient R_∞. Taking the quasistatic limit of the eigenvalue equation (11), we form

$$\begin{bmatrix} (\chi_\infty - \chi_1)^2 & (\chi_1^2 - \chi_\infty^2) \\ -(\chi_1^2 - \chi_\infty^2) & (\chi_\infty + \chi_1)^2 \end{bmatrix}\begin{bmatrix} f^- \\ f^+ \end{bmatrix} = \begin{bmatrix} 0 \\ 0 \end{bmatrix}, \tag{71}$$

the null space of which characterizes the forward and backward propagating eigenstates. Selecting the null vector corresponding to the forward propagating wave associated with $\beta_0 = +\chi_\infty$, we calculate

TABLE IV. Dynamic extrapolated estimate of ε_{eff} for $H_{\parallel}$ polarization.

	λ/d				
n	25	50	100	200	400
1	1.67 128	1.667 43	1.666 48	1.666 25	1.666 19
2	0	1.663 59	1.665 53	1.666 01	1.666 13
3	0	0	1.666 18	1.666 17	1.666 17
4	0	0	0	1.666 17	1.666 17
5	0	0	0	0	1.666 17

TABLE V. Static extrapolated estimate of ε_{eff} for $H_{\parallel}$ polarization.

	λ/d				
n	25	50	100	200	400
1	1.671 83	1.667 58	1.666 52	1.666 26	1.666 19
2	0	1.663 33	1.665 46	1.665 99	1.666 12
3	0	0	1.666 17	1.666 17	1.666 17
4	0	0	0	1.666 17	1.666 17
5	0	0	0	0	1.666 17

$$R_{\infty}=\frac{\chi_1-\chi_{\infty}}{\chi_1+\chi_{\infty}}, \tag{72}$$

the Fresnel reflection coefficient corresponding to propagation into a unbounded medium of permittivity ε_{∞}.

The result (72) is the basis of the ''electrostatic'' method of calculating the effective permittivity of two- and three-dimensional photonic crystals. Here, the specular order of $\mathbf{R}_{\infty}$ is used to define a reflection coefficient $r=\mathbf{R}_{00}^{\infty}$, for $E_{\parallel}$ and $H_{\parallel}$ polarizations, respectively, from which we may calculate the ''electrostatic'' refractive index and infer an effective permittivity according to

$$n_{\text{stat}}=\frac{1-r}{1+r}, \quad \varepsilon_{\text{eff}}=n_{\text{stat}}^2 \tag{73}$$

for normal incidence ($\alpha_0=0$). An alternative method estimates the ''dynamic'' refractive index from the slope of the acoustic band. Again for normal incidence, we have $\mu=\exp(i\beta_0 d_y)$ and we define [8]

$$n_{\text{dyn}}=\frac{d\beta_0}{dk}\approx\frac{\beta_0}{k}, \quad \varepsilon_{\text{eff}}=n_{\text{dyn}}^2. \tag{74}$$

The estimates of ε_{eff} are functions of the wave number k,

$$\varepsilon_{\text{eff}}(k)=\varepsilon_0+\varepsilon_1 k+\varepsilon_2 k^2+\varepsilon_3 k^3+\cdots, \tag{75}$$

and we compute a sequence

$$\{\varepsilon_{\text{eff}}(k_0),\varepsilon_{\text{eff}}(k_0/2),\varepsilon_{\text{eff}}(k_0/4),\ldots\},$$

to which we apply Richardson extrapolation [30] to accelerate the convergence of the estimates to the static limit $\varepsilon_{\text{eff}}(0)$.

In Tables IV and V we show the five step extrapolation table for the calculation of the effective permittivity of a square symmetric lattice of dielectric cylinders of normalized radius $a/d=0.3$ and refractive index $\nu=3.0$, subject to an electric field oriented perpendicular to the axes of the cylinders ($H_{\parallel}$ polarization). This calculation exploits scattering matrices from the $H_{\parallel}$ diffraction problem, in which we have preserved only the five most significant plane wave diffracted orders $\{-2,-1,0,1,2\}$. We see that excellent convergence is obtained in five steps commencing with a normalized wavelength of $\lambda/d=25.0$. The extrapolated limit of $\varepsilon_{\text{eff}}=1.666\,17$ is to be compared with the true value of $\varepsilon_{\text{MP}}=1.666\,16$ obtained from the Rayleigh multipole theory of electrostatics, and its well-known dipole approximation, the Maxwell-Garnett formula $\varepsilon_{\text{MG}}=1.664\,82$. We have also applied the method to the calculation of the permittivity of an array with an electric field oriented parallel (i.e., the $E_{\parallel}$ problem) to the cylinders and found the convergence to the Wiener [29], or linear mixing formula, to be extremely rapid.

The $E_{\parallel}$ and $H_{\parallel}$ problems are distinguished by a marked dependence on the interlayer coupling mechanism. To investigate this, we truncated the scattering matrices at order $p\in\{0,1,2,\ldots,5\}$ and calculated ε_{eff} in each case. The results are shown in Table VI and reveal that for $E_{\parallel}$ polarization convergence is achieved by the inclusion of only the specular order in the scattering matrices, while for $H_{\parallel}$ polarization, convergence requires the inclusion of both specular and evanescent orders. This agrees with previous work [31] in which it was shown that long wavelength homogenization was dominated by the monopole term in the cylindrical harmonic field expansion that is related directly to the specular plane wave order. In contrast, homogenization for $H_{\parallel}$ polarization is dictated by the dipole term, the expansion of which in plane waves requires both specular and evanescent orders.

V. LONG WAVELENGTH FORMULATION

For sufficiently long wavelengths, the coupling between layers is dominated by the specular ($p=0$) order that is the sole propagating channel. Provided that the layers are sufficiently separated and that evanescent coupling is negligible, the scattering matrices can be replaced by a single scalar element corresponding to input and output in the zeroth order

TABLE VI. Comparison of the effect of different interlayer coupling mechanisms on ε_{eff} for both $E_{\parallel}$ and $H_{\parallel}$ polarization number of plane wave orders p. Here, scattering matrices contain the orders $\{-p,-p+1,\ldots,0,1,\ldots,p\}$.

	$\varepsilon_{\text{eff}}(0)$	
p	$E_{\parallel}$ polarization	$H_{\parallel}$ polarization
0	5.241 15	1.676 09
1	5.241 15	1.666 20
2	5.241 15	1.666 17
3	5.241 15	1.666 17
4	5.241 15	1.666 17
5	5.241 15	1.666 17

channel. In what follows, we initially derive results for lossless structures and extend them to highly conducting gratings at long wavelengths.

As we have seen, a layered media is characterized by two key quantities, the eigenvalues μ and the reflection coefficient R_∞. Here we demonstrate their close interrelationship, deriving a simple formula that predicts the location of band gaps at long wavelengths, for which only the specular diffracted order is propagating.

We denote by R and T the single layer reflection and transmission coefficients corresponding to unit incidence from above, and by R' and T' the corresponding coefficients for incidence from below. From the reciprocity theorem, the forward and backward transmission coefficients are identical, i.e., $T=T'$. While $R\neq R'$ in general, a relationship between them can be derived using the principle of time reversal. We consider an initial problem corresponding to incidence from above and, under time reversal, we return the two outgoing fields—a wave of amplitude $\overline{R}$ from above, and one of amplitude $\overline{T}$ from below. These form an upward going wave of amplitude $R\overline{R}+T\overline{T}$ above and a downward going wave of amplitude $T\overline{R}+R'\overline{T}$ below. From the principle of time reversal, it follows that

$$R\overline{R'}+T\overline{T}=1, \tag{76}$$

$$T\overline{R}+R'\overline{T}=0. \tag{77}$$

By considering a second problem associated with unit incidence from below and, by returning its outgoing waves, it follows similarly that

$$R'\overline{R}+T\overline{T}=1, \tag{78}$$

$$T\overline{R'}+R\overline{T}=0. \tag{79}$$

From Eqs. (76) and (78) it follows that $|R|=|R'|$ and from Eqs. (77) and (79) we see that

$$\exp(2i\psi_T)=-\exp[i(\psi_R+\psi_{R'})], \tag{80}$$

where $\psi_T=\arg T$, $\psi_R=\arg R$, and $\psi_{R'}=\arg R'$.

We commence with the eigenvalue equation (12) which, in the scalar approximation, reduces to a quadratic equation

$$\mu^2-2b\mu+1=0, \tag{81}$$

$$b=\frac{T^2-RR'+1}{2T}=\frac{\cos\psi_T}{|T|}, \tag{82}$$

a result that follows from Eq. (80). Since b is real for lossless structures, it follows that propagating modes may occur as conjugate pairs of eigenvalues μ of unit magnitude provided that $b^2\leqslant 1$, and as evanescent modes associated with reciprocal pairs of real eigenvalues for $b^2>1$.

We next consider R_∞ and R'_∞, observing that the correspondence between them and the respective eigenvalues μ and $\mu'=1/\mu$ is given by the scalar forms of Eqs. (53) and (54):

$$R_\infty=\frac{1-T\mu^{-1}}{R'}, \tag{83}$$

$$R'_\infty=\frac{1-T\mu^{-1}}{R}, \tag{84}$$

so that $R'R_\infty=RR'_\infty$. It may be shown that these forms are the fixed points of the usual recurrence relations that are used to calculate the reflection coefficient of a stack properties in a recursive or inductive manner [15]. Now, from the respective pairs of spectral forms (53) and (55), and (54) and (56), we may derive quadratic equations in R_∞ and R'_∞ that are linked according to

$$R_\infty=\tilde{R}_\infty\exp[i(\psi_R-\psi_{R'})/2], \tag{85}$$

$$R'_\infty=\tilde{R}_\infty\exp[-i(\psi_R-\psi_{R'})/2], \tag{86}$$

where $\tilde{R}_\infty$ satisfies the quadratic equation

$$\tilde{R}_\infty^2-2a\tilde{R}_\infty+1=0, \tag{87}$$

$$a=-\frac{T^2-RR'-1}{2|R|}\exp-i(\psi_R+\psi_{R'})/2$$
$$=\cos[(\psi_R+\psi_{R'})/2]/|R|. \tag{88}$$

From Eqs. (82) and (88) it follows that

$$b^2-1=\frac{|R|^2}{|T|^2}(1-a^2), \tag{89}$$

implying that for propagating states (i.e., $b^2\leqslant 1$, $a^2\geqslant 1$) $\tilde{R}_\infty$ must be the minimum magnitude real solution of Eq. (87). Correspondingly, for evanescent or band gap states, $\tilde{R}_\infty$ is a complex number of unit magnitude and, in either case, it follows readily that $R_\infty=\overline{R'_\infty}$. We also observe that the scalar result $|R_\infty|=1$ that holds in a band gap shows that the crystal behaves as a mirror. Its generalization, to full scattering matrices, can be shown to be

$$\mathbf{R}_\infty^H\mathbf{I}_r\mathbf{R}_\infty=\mathbf{I}_r+i\mathbf{I}_e\mathbf{R}_\infty-i\mathbf{R}_\infty^H\mathbf{I}_e, \tag{90}$$

where $\mathbf{I}_r$ is a diagonal matrix that selects the propagating plane wave orders Ω_r (i.e., $[\mathbf{I}_r]_{pq}=\delta_{pq}$ for $p\in\Omega_r$) and $\mathbf{I}_e$ is the corresponding diagonal matrix that selects the evanescent plane wave orders (i.e., $\mathbf{I}_r+\mathbf{I}_e=\mathbf{I}$). The derivation follows the treatment of Botten *et al.* [16] and has been verified numerically.

The transition from propagation to evanescence delimits the band gap and occurs when $|a|=|b|=1$. That is, when

$$|R|=\cos(\psi_R+\psi_{R'})/2 \quad \text{or} \quad |T|=\cos\psi_T. \tag{91}$$

While these derivations assume lossless media, the results also apply to highly conducting (lossy) materials, as is evident from Fig. 9 that displays the reflectance ($\mathcal{R}$), transmittance ($\mathcal{T}$), and absorptance ($\mathcal{A}$), defined as [15]

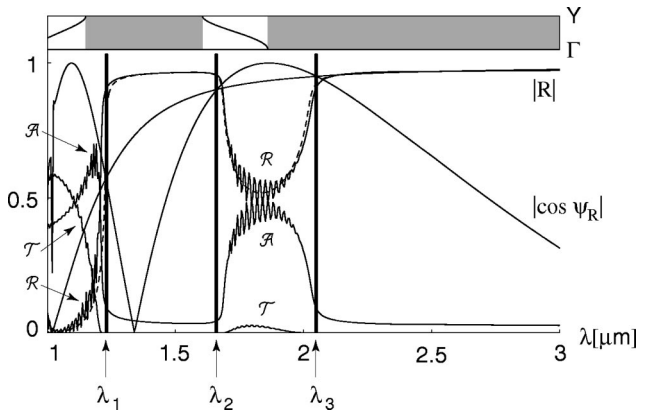

FIG. 9. Reflectance ($\mathcal{R}$), transmittance ($\mathcal{T}$), and absorptance ($\mathcal{A}$) for $E_\parallel$ polarization, for a stack of 25 cylinder gratings in vacuum, forming a square array ($d_x=d_y=1\ \mu$m, $s_x=0$). The cylinders are made from gold and have a radius $a=0.20\ \mu$m. The dashed curve shows the reflectance $|R_\infty|^2$ of a semi-infinite stack. The vertical thick lines at $\lambda_1=1.23\ \mu$m, $\lambda_2=1.66\ \mu$m, and $\lambda_3=2.05\ \mu$m, determined by the intersections $|R|=|\cos\psi_R|$, mark the edges of the partial gaps for the stack of gratings. The inset, above the plot, shows the region ΓY (see Fig. 5) of the photonic band diagram for a square array ($d_x=d_y=1\ \mu$m, $s_x=0$) of perfectly conducting cylinders ($a/d_x=1$) in vacuum, with the gray rectangles specifying the partial gaps.

$$\mathcal{R}=|R|^2, \quad \mathcal{T}=|T|^2, \quad \mathcal{A}=1-\mathcal{R}-\mathcal{T}, \tag{92}$$

of a 25-layer square symmetric stack of gold cylinders of period $d_x=1.0\ \mu$m and radius $a=0.2\ \mu$m. For this application we used the dielectric function of gold obtained by interpolating the experimental data from Ref. [32]. We see that the boundaries of the band gaps are well approximated by Eq. (91) and note that these are slightly displaced from those of the corresponding perfectly conducting structure (i.e., a structure consisting of perfectly conducting cylinders leading to Dirichlet and Neumann boundary conditions for the $E_\parallel$ and $H_\parallel$ field problems, respectively), shown in the band diagram at the top of the figure.

Also shown in Fig. 9 is the reflectance of the semi-infinite array $|R_\infty|^2$ [calculated according to Eq. (83)] that closely follows the actual data ($\mathcal{R}$) for the 25 layer structure. Observe, in the propagation band region for $1.66\lesssim\lambda\lesssim2.05$, that the transmittance ($\mathcal{T}$) is quite low, and that the reflectance ($\mathcal{R}$) is reduced by enhanced or anomalous absorptance ($\mathcal{A}$) [33]. In contrast, in the second propagation band region ($1\lesssim\lambda\lesssim1.23$) the transmittance is very low, while the reflectance and absorptance are almost equal.

Finally, we consider the long wavelength form of the transmission coefficient T_n using Eq. (60):

$$T_n=\frac{(1-|R_\infty|^2)\mu^n}{1-|R_\infty|^2\mu^{2n}}. \tag{93}$$

Clearly, $|T_n|$ maximizes at 1 when $\mu^{2n}=1$ and minimizes when $\mu^{2n}=-1$, the latter value defining an envelope, touched by the transmission minima, whose form is

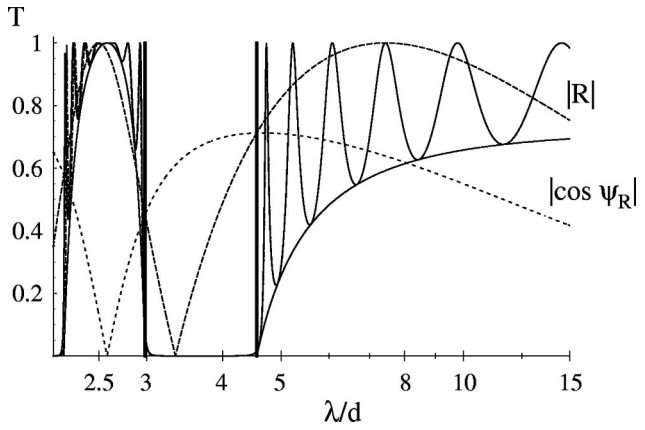

FIG. 10. $E_\parallel$ polarization: envelope of the transmittance and the positions of the partial band gaps, delimited by $|R|=|\cos\psi_R|$, for a stack of eight cylinder gratings in vacuum, forming a square array ($d_x=d_y=1\ \mu$m, $s_x=0$). The cylinders are of radius $a/d_x=0.3$ and refractive index $\nu_{cyl}=3$. The vertical thick lines, determined by the intersections $|R|=|\cos\psi_R|$ (dashed curves), mark the edges of the partial gaps for the stack of gratings. The envelope that touches the interference transmittance minima is given by Eq. (95).

$$|T_{\rm env}|=\frac{1-|R_\infty|^2}{1+|R_\infty|^2}=-1+\frac{1}{a|R_\infty|}. \tag{94}$$

For up-down symmetric layers, it follows from Eqs. (85) and (86) that

$$|T_{\rm env}|^2=1-\frac{1}{a^2}=1-\frac{|R|^2}{\cos^2\psi_R}. \tag{95}$$

Figure 10 displays the envelope and the position of the band gap delimited by $|R|=|\cos\psi_R|$, coinciding with the base of the envelope. We note that the positions of the transmission maxima and minima are given by

$$\cos(2\psi_R)=|R|^2-|T|^2\cos\arg(\kappa_j), \tag{96}$$

where ψ_R is the phase of the reflected field and κ denotes the nth roots of 1, in the case of the fringe maxima, and the nth roots of -1, for the fringe minima. These roots are

$$\kappa_j^{\max}=\exp\left[i\frac{2j\pi}{n}\right], \tag{97}$$

$$\kappa_j^{\min}=\exp\left[i\frac{(2j+1)\pi}{n}\right], \tag{98}$$

for $j=0,1,\ldots,n-1$. In general, however, Eq. (96) has no closed form solution as the reflected and transmitted efficiencies are functions of wavelength, as is the phase of the reflected field $\psi_R(\lambda)=\psi_R^0(\lambda)+2\pi d_y/\lambda$, where ψ_R^0 is the reflected field phase relative to phase origin through $y=0$.

VI. INFERENCE OF TWO-DIMENSIONAL LATTICE SUMS

Thus far, the eigenvalue method has been used to calculate band structures from plane wave scattering matrices. In this section, we show that it can be also applied to the waveguide modal fields for problems formulated with the Rayleigh method to derive computationally important relationships between the lattice sums of the two-dimensional lattice and those of the constituent grating.

We follow the treatment and nomenclature of [15] and consider a cylinder grating of period d_x with a single cylinder per period. In the vicinity of each cylinder, the field is expanded in cylindrical harmonics

$$V(\mathbf{r})=\sum_{n=-\infty}^{\infty}[A_nJ_n(kr)+B_nH_n^{(1)}(kr)]e^{in\theta}, \tag{99}$$

where k denotes the wave number from the Helmholtz differential operator ∇^2+k^2. At the surface of each cylinder, the physical boundary conditions impose relationships [15] of the form

$$A_m=-M_mB_m. \tag{100}$$

Following [15] and applying Green's theorem over the unit cell, we derive the Rayleigh identity that expresses the coefficients of the regular part of the field (A_n) in terms of the coefficients of sources on all the other cylinders (B_n) and sources at infinity (i.e., plane waves). Thus,

$$A_n=\sum_{m=-\infty}^{\infty}S_{n-m}^GB_m + \sum_{p=-\infty}^{\infty}\chi_p^{-1/2}[(-1)^ne^{-in\theta_p}\delta_p^-+e^{in\theta_p}\delta_p^+], \tag{101}$$

where the S_l^G denote the grating lattice sums

$$S_l^G=\sum_{n\neq 0}H_l^{(1)}(k|n|d_x)e^{-il\arg(n)}e^{i\alpha_0nd_x}, \tag{102}$$

that specify the multipole contributions arising from sources at the centers of the cylinders. The final term in Eq. (101) comprises two plane wave sources respectively incident on the grating from above $\{\delta_p^-\}$ and below $\{\delta_p^+\}$, where the $\delta_p^\pm$ are coefficients in plane wave expansions of the form

$$\sum\ \chi_p^{-1/2}\delta_p^\pm\exp[i(\alpha_px\pm\chi_py)]. \tag{103}$$

Substituting the boundary conditions (100) into the field identity (101), and recasting the expression in matrix form we have

$$(\mathbf{S}^G+\mathbf{M})\mathbf{B}=-(\mathbf{UJ}\boldsymbol{\chi}^{-1/2}\boldsymbol{\delta}^-+\mathbf{K}\boldsymbol{\chi}^{-1/2}\boldsymbol{\delta}^+), \tag{104}$$

where

$$\mathbf{S}^G=[S_{nm}^G]=[S_{n-m}^G],\quad \mathbf{U}=\mathrm{diag}[(-1)^n],$$

$$\mathbf{J}=[J_{np}]=[e^{-in\theta_p}],\quad \mathbf{K}=[K_{np}]=[e^{in\theta_p}],$$

$$\boldsymbol{\chi}=\mathrm{diag}[\chi_p],\quad \boldsymbol{\delta}^\pm=[\delta_p^\pm].$$

The outgoing fields above and below the grating may be reconstructed in terms of the incident plane wave fields and fields radiated by the cylinders [15]. Above the grating, the upward going field has components

$$f_p^+=\delta_p^++\frac{2}{id_x}\chi_p^{-1/2}\sum_{n=-\infty}^{\infty}B_ne^{-in\theta_p}, \tag{105}$$

with the first term denoting the specular transmission of the incident field from below, and the second term representing the diffracted field. In matrix form, the outgoing plane wave fields above and below the grating are, respectively,

$$\mathbf{f}^+=\boldsymbol{\delta}^++\frac{2}{id_x}\boldsymbol{\chi}^{-1/2}\mathbf{J}^T\mathbf{B} \tag{106}$$

and

$$\mathbf{f}^-=\boldsymbol{\delta}^-+\frac{2}{id_x}\boldsymbol{\chi}^{-1/2}\mathbf{K}^T\mathbf{UB}. \tag{107}$$

The modes of a general two-dimensional lattice are now formed by imposing the Bloch condition, which requires that

$$\begin{aligned}\mu\exp[i(\alpha_ps_x/2-\chi_pd_y/2)]\delta_p^- &= \exp[-i(\alpha_ps_x/2-\chi_pd_y/2)]f_p^-,\\ \mu\exp[i(\alpha_ps_x/2+\chi_pd_y/2)]f_p^+ &= \exp[-i(\alpha_ps_x/2+\chi_pd_y/2)]\delta_p^+\end{aligned} \tag{108}$$

for the pth plane wave coefficient, taking into account the need to adjust plane wave phase origins in accordance with Sec. II A. In matrix form, we have

$$\mathbf{f}^-=\mu\mathbf{Q}^2\mathbf{P}^{-2}\boldsymbol{\delta}^-,\quad \mathbf{f}^+=\mu^{-1}\mathbf{Q}^{-2}\mathbf{P}^{-2}\boldsymbol{\delta}^+ \tag{109}$$

and, substituting these into Eqs. (106) and (107), we express the eigenincident fields $\boldsymbol{\delta}^\pm$ in terms of the source coefficients **B**. In turn, these are substituted into the field identity (105) to yield a homogeneous system that is the Rayleigh identity for the two-dimensional array:

$$\left\{\mathbf{S}^G+\frac{2}{d}\left[\mathbf{UJ}\frac{\boldsymbol{\chi}^{-1}}{\mu\mathbf{QP}^{-1}-\mathbf{I}}\mathbf{K}^T\mathbf{U}+\mathbf{K}\frac{\boldsymbol{\chi}^{-1}}{\mu^{-1}\mathbf{Q}^{-1}\mathbf{P}^{-1}-\mathbf{I}}\mathbf{J}^T\right]+\mathbf{M}\right\}\mathbf{B}=\mathbf{0}, \tag{110}$$

or

$$[\mathbf{S}^G+\Delta\mathbf{S}+\mathbf{M}]\mathbf{B}=\mathbf{0}. \tag{111}$$

This form (111) of the Rayleigh identity must be equivalent to the alternative form in which the modes of lattice are expressed directly in terms of the array lattice sums [8]

$$[\mathbf{S}^A+\mathbf{M}]\mathbf{B}=\mathbf{0}, \tag{112}$$

with the boundary condition matrix **M** being the same in both cases. Here,

$$\mathbf{S}^A=[S^A_{nm}]=[S^A_{n-m}], \tag{113}$$

where

$$S^A_l=\sum_{(n,m)}{}' H^{(1)}_l(k|\mathbf{l}_{nm}|)\exp[-il\arg(\mathbf{l}_{nm})]e^{i\mathbf{k}_0\cdot\mathbf{l}_{nm}}, \tag{114}$$

and the prime means that the term $(n,m)=(0,0)$ is excluded from the sum. By subtracting Eq. (111) from Eq. (112), we have

$$[\mathbf{S}^A-(\mathbf{S}^G+\Delta\mathbf{S})]\mathbf{B}=\mathbf{0}, \tag{115}$$

with the coefficient matrix in Eq. (115) depending solely on the lattice geometry parameters and not involving material properties such as cylinder radius or electric permittivity. Accordingly, we deduce that Eq. (115) must hold for all **B** and thus

$$\mathbf{S}^A=\mathbf{S}^G+\Delta\mathbf{S}. \tag{116}$$

While the derivation has involved plane wave coupling between layers, the final form of the result is independent of the cylinder radius and should thus be valid for all lattices, including those with interpenetrating layers for which plane wave coupling between layers is no longer appropriate.

Finally, we infer expressions for the array lattice sums S^A_l in terms of grating lattice sums S^G_l and correction terms ΔS_l:

$$S^A_l=S^G_l+\Delta S_l, \tag{117}$$

where

$$\Delta S_l=\frac{2}{d}\sum_{p=-\infty}^{\infty}\frac{1}{\chi_p}\left[\frac{e^{il\theta_p}}{\mu^{-1}Q_p^{-1}P_p^{-1}-1}+\frac{(-1)^l e^{-il\theta_p}}{\mu Q_p P_p^{-1}-1}\right]. \tag{118}$$

For p sufficiently large the term $\exp(i\theta_p)=(\chi_p+i\alpha_p)/k$ becomes $\exp(i\theta_p)\sim i2\pi|p|[1+\mathrm{sign}(p)]/(kd)+\mathcal{O}(k^2)$. Correspondingly, $|P_p^{-1}|\sim\exp(2\pi|p|kd)$ and so the series in Eq. (118) are exponentially convergent. Recasting the denominator of the terms in Eq. (118) as geometric series, we obtain

$$\Delta S_n=\frac{2}{d}\left[\sum_{l=1}^{\infty}\mu^l\sum_{p=-\infty}^{\infty}\chi_p^{-1}e^{in\theta_p}\exp\{il(\alpha_p s_x+\chi_p d_y)\}\right.$$
$$+(-1)^n\sum_{l=1}^{\infty}\mu^{-l}\sum_{p=-\infty}^{\infty}\chi_p^{-1}e^{-in\theta_p}$$
$$\left.\times\exp\{il(-\alpha_p s_x+\chi_p d_y)\}\right], \tag{119}$$

and immediately, from the presence of μ^l and μ^{-l}, it follows that the terms in the series of Eq. (119) represent contributions to the array lattice sums from grating layers displaced vertically from the central grating by $\pm ld_y$.

This heuristic derivation of the relationship between array and grating lattice sums has also been supplemented by a rigorous analytic demonstration from first principles [34]. The relationship is of considerable significance computationally as it increases the speed of evaluation of array lattice sums (116) by a factor of at least 10 over the original technique [35,36].

VII. CONCLUSIONS

This paper has presented a comprehensive discussion of the Bloch technique, which enables one to go from the scattering properties of a grating to the modes that propagate in any array comprising a stack of gratings. The method is accurate, computationally robust as well as of enhanced efficiency, in comparison with both our Rayleigh multipole theory for arrays [20] and plane wave methods [2,3].

Unlike plane wave techniques, the method is also well suited to the analysis of arrays and lattices containing lossy, metallic components. In such cases, the eigenvalues are complex numbers and problems to be addressed in future relate more to their visualization than calculation.

The analytic treatment of scattering matrices of finite stacks has led to a fundamental new quantity $\mathbf{R}_\infty$ that is the scattering matrix for a semi-infinite array and is deduced directly from the modal eigenproblem. Indeed, $\mathbf{R}_\infty$ can be used as a ''black box'' to encapsulate the properties of a substrate comprising an array of arbitrarily large thickness, as arises in the treatment of photonic crystal gratings [37].

The technique is not limited to the connection between gratings and arrays and, in future work, we will explore the connection between scattering from a monolayer of spheres, and modes that propagate in lattices composed of such monolayers. Again, the grating need not contain one scatterer per unit cell, and so we may investigate the modes that propagate in crystal structures of quite general form in this way. The method has also elucidated the connection between monolayers and arrays constructed from them in the form of relationships between their lattice sums.

ACKNOWLEDGMENTS

This work has been supported by the Australian Research Council. Helpful discussions with J. Pendry, D. Maystre, G. Tayeb, and S. Enoch are acknowledged.

APPENDIX: ENERGY FLOW AND GROUP VELOCITY

Here, we relate the group velocity and energy flux to derive the result

$$\nabla_{\mathbf{k}_0}\omega = \frac{c^2}{\omega}\frac{\boldsymbol{\mathcal{E}}_F}{\mathcal{E}_D}, \tag{A1}$$

where $\boldsymbol{\mathcal{E}}_F$ denotes the vector energy flux through the unit cell and $\mathcal{E}_D$ denotes the electric energy density per unit cell. The derivation given here is for $E_\parallel$ polarization. A similar treatment yields the same result for $H_\parallel$ polarization. We derive one component of the group velocity by considering the limit of an energy integral associated with two field problems, and infer from this the general form of the result.

We begin by defining two field problems for fields u and u', respectively, satisfying Helmholtz equations

$$[\nabla^2 + k^2\varepsilon(\mathbf{r})]u = 0, \tag{A2}$$

$$[\nabla^2 + k'^2\varepsilon(\mathbf{r})]u' = 0, \tag{A3}$$

and Bloch conditions

$$u(\mathbf{r} + m\mathbf{e}_1 + n\mathbf{e}_2) = \nu^m\mu^n u(\mathbf{r}), \tag{A4}$$

$$u'(\mathbf{r} + m\mathbf{e}_1 + n\mathbf{e}_2) = \nu^m\mu'^n u'(\mathbf{r}), \tag{A5}$$

where $\nu = \exp(i\mathbf{k}_0\cdot\mathbf{e}_1)$, $\mu = \exp(-i\mathbf{k}_0\cdot\mathbf{e}_2)$, and $\mu' = \exp(-i\mathbf{k}_0'\cdot\mathbf{e}_2)$, with $\mathbf{k}_0 = (\alpha_0, \beta_0)$ and $\mathbf{k}_0' = (\alpha_0, \beta_0')$.

An application of Green's Theorem around a unit parallelogram cell U, with sides defined by the vectors $\mathbf{e}_1$ and $\mathbf{e}_2$, enables us to derive

$$\int\int_U u\nabla^2\overline{u'} - \overline{u'}\nabla^2 u\, dA = \left(\int_{\Gamma_+} dx - \int_{\Gamma_-} dx\right) u\frac{\partial\overline{u'}}{\partial y} - \overline{u'}\frac{\partial u}{\partial y}. \tag{A6}$$

In Eq. (A6), the contours $\Gamma_\pm$ are the upper and lower horizontal boundaries of the parallelogram cell (parallel to the vector $\mathbf{e}_1$). Quasiperiodicity in the direction $\mathbf{e}_1$ cancels contributions to the line integral from the sides of the parallelogram that are parallel to $\mathbf{e}_2$. Applying the Helmholtz equations (A3) and the quasiperiodicity equations (A5) in Eq. (A6) and taking limits as $k' \to k$, $\beta_0' \to \beta_0$ in yields

$$\lim_{k'\to k}\frac{k^2 - k'^2}{\beta_0 - \beta_0'} = \frac{-id_y\int_{\Gamma_+}[u\partial\overline{u}/\partial y - \overline{u}\partial u/\partial y]dx}{\int\int_U \varepsilon(\mathbf{r})|u(\mathbf{r})|^2 dA}. \tag{A7}$$

Following the treatment of [16], the numerator of the right-hand side of Eq. A7 may be shown to be

$$2id_x\boldsymbol{\mathcal{E}}_{F,y} = 2id_x\left[\sum_{p\in\Omega_r}(|f_p^-|^2 - |f_p^+|^2) - 2\,\mathrm{Im}\sum_{p\in\Omega_r} f_p^-\overline{f_p^+}\right], \tag{A8}$$

where $\boldsymbol{\mathcal{E}}_{F,y}$ is downward energy flux in the y direction. Correspondingly, the denominator of right-hand side of Eq. (A7) is $\mathcal{E}_D\,dxdy$, where $\mathcal{E}_D$ denotes the electric energy density per unit cell. It then follows from Eq. (A7) that the y component of the group velocity is given by

$$\frac{\partial k}{\partial\beta_0} = \frac{\mathcal{E}_{F,y}}{k\mathcal{E}_D}. \tag{A9}$$

The same arguments yield an analogous expression for the x component of the group velocity, from which the result in Eq. (A1) follows.

[1] J. P. Dowling, H. Everitt, and E. Yablonovitch, web page http://home.earthlink.net/~jpdowling/pbgbib.html

[2] K. M. Ho, C. T. Chan, and C. M. Soukoulis, Phys. Rev. Lett. **65**, 3152 (1990).

[3] K. M. Leung and Y. F. Liu, Phys. Rev. Lett. **65**, 2646 (1990).

[4] J. B. Pendry and A. MacKinnon, Phys. Rev. Lett. **69**, 2772 (1992).

[5] J. B. Pendry, J. Phys.: Condens. Matter **8**, 1085 (1996).

[6] C. T. Chan, Q. L. Yu, and K. M. Ho, Phys. Rev. B **51**, 16 635 (1995).

[7] N. Stefanou, V. Karathanos, and A. Modinos, J. Phys.: Condens. Matter **4**, 7389 (1992).

[8] N. A. Nicorovici, R. C. McPhedran, and L. C. Botten, Phys. Rev. E **52**, 1135 (1995).

[9] N. A. Nicorovici, R. C. McPhedran, and L. C. Botten, Phys. Rev. Lett. **75**, 1507 (1995); **86**, 3211 (2001); **86**, 3212 (2001).

[10] E. G. McRae, Surf. Sci. **11**, 479 (1968); **11**, 492 (1968).

[11] B. Gralak, S. Enoch, and G. Tayeb, J. Opt. Soc. Am. A **17**, 1012 (2000).

[12] *Electromagnetic Theory of Gratings*, edited by R. Petit, Topics in Current Physics (Springer-Verlag, Berlin, 1980), Vol. 22, pp. 1–52.

[13] *Selected Papers on Diffraction Gratings*, edited by D. Maystre (SPIE Optical Eng. Press, Bellingham, Washington, 1993).

[14] C. Kittel, *Introduction to Solid State Physics* (Wiley, New York, 1966).

[15] L. C. Botten, N. A. Nicorovici, A. A. Asatryan, R. C. McPhedran, C. M. de Sterke, and P. A. Robinson, J. Opt. Soc. Am. A **17**, 2165 (2000).

[16] L. C. Botten, N. A. Nicorovici, A. A. Asatryan, R. C. McPhedran, C. M. de Sterke, and P. A. Robinson, J. Opt. Soc. Am. A **17**, 2177 (2000).

[17] J. M. Elson and P. Tran, J. Opt. Soc. Am. A **17**, 2983 (1999).

[18] L. Li, J. Opt. Soc. Am. A **13**, 1024 (1996).

[19] M. C. Hutley, *Diffraction Gratings* (Academic, New York, 1982).

[20] R. C. McPhedran, N. A. Nicorovici, and L. C. Botten, J. Electromagn. Waves Appl. **11**, 981 (1997).

[21] R. Petit and M. Cadilhac, Comptes, C. R. Seances Acad.

Sci., Ser. B **262**, 468 (1966), reprinted in [13]. See also Chap. 2 of [12].
[22] D. Maystre and M. Cadilhac, J. Math. Phys. **26**, 2201 (1985).
[23] A. G. Kyurkchan, B. Yu. Sternin, and V. E. Shatalov, Usp. Fiz. Nauk. **166**, 1285 (1996).
[24] R. H. Bates, IEEE Trans. Microwave Theory & Tech. **23**, 605 (1975).
[25] A. R. Parker, R. C. McPhedran, D. R. McKenzie, L. C. Botten, and N. A. Nicorovici, Nature (London) **409**, 36 (2001).
[26] R. C. McPhedran, N. A. Nicorovici, D. R. McKenzie, L. C. Botten, A. R. Parker, and G. W. Rouse, Aust. J. Phys. (to be published).
[27] C. L. Stephen and C. D. Meyer, *Generalized Inverses of Linear Transformations* (Dover Publications, New York, 1991).
[28] M. Born and E. Wolf, *Principles of Optics*, 6th ed. (Pergamon Press, Oxford, 1980), p. 343.
[29] O. Wiener, Abh. Math. Phys. Kl. Königl. Säch Gess. Wiss. **32**, 509 (1912).
[30] W. H. Press, S. A. Teukolsky, W. T. Vetterling, and B. P. Flannery, *Numerical Recipes in Fortran 77*, Second Edition (Cambridge University Press, New York, 1997).
[31] A. A. Asatryan, P. A. Robinson, L. C. Botten, R. C. McPhedran, N. A. Nicorovici, and C. M. de Sterke, Phys. Rev. E **60**, 6118 (1999).
[32] E. D. Palik, *The Handbook of Optical Constants of Solids* (Academic, New York, 1993).
[33] R. C. McPhedran, N. A. Nicorovici, L. C. Botten, C. M. de Sterke, P. A. Robinson, and A. A. Asatryan, Opt. Commun. **168**, 47 (1999).
[34] R. C. McPhedran, N. A. Nicorovici, L. C. Botten, and K. A. Grubits, J. Math. Phys. **41**, 7808 (2000).
[35] S.K. Chin, N.A. Nicorovici, and R.C. McPhedran, Phys. Rev. E **49**, 4590 (1994).
[36] R. C. McPhedran, N. A. Nicorovici, L. C. Botten, and Bao Ke-Da, in *Wave Propagation in Complex Media*, edited by G. Papanicolau, The IMA Volumes in Mathematics and Its Applications (Springer-Verlag, New York, 1997), Vol. 96, pp. 155-186.
[37] D. Maystre, Opt. Express **8**, 209 (2001).